5-2021

Rare Earth-Doped Glass-Ceramic Scintillators as X-Ray Flat Panel Detector Substrates

Austin M. Thomas
The University of Tennessee, athoma81@vols.utk.edu

To the Graduate Council:

I am submitting herewith a thesis written by Austin M. Thomas entitled "Rare Earth-Doped Glass-Ceramic Scintillators as X-Ray Flat Panel Detector Substrates." I have examined the final electronic copy of this thesis for form and content and recommend that it be accepted in partial fulfillment of the requirements for the degree of Master of Science, with a major in Biomedical Engineering.

Jacqueline A. Johnson, Major Professor

We have read this thesis and recommend its acceptance:

Jacqueline A. Johnson, Russell L. Leonard, Feng-Yuan Zhang

Accepted for the Council:
Dixie L. Thompson

Vice Provost and Dean of the Graduate School

(Original signatures are on file with official student records.)

Rare Earth-Doped Glass-Ceramic Scintillators as X-Ray Flat Panel Detector Substrates

A Thesis Presented for the
Master of Science
Degree
The University of Tennessee, Knoxville

Austin Michael Thomas
May 2021

ACKNOWLEDGEMENTS

I would like to begin by giving my thanks to my academic advisor, Dr. Jacqueline Johnson for her guidance during the past three years. She has been a great source of guidance, has challenged me to become a better researcher and has been very patient with me through this entire endeavor.

I would also like to thank Dr. Lee Leonard, who has helped me almost every step of the way through my research. Lee taught me a great deal both in the lab and out of it and I truly appreciate all the help he has given me.

I would like to thank Dr. Feng Yuan Zhang, who participated on my thesis committee. I appreciate the questions asked during my defense, as well as the support he has given me.

I have really enjoyed my time here at UTSI. Everyone here has always been very supportive and helpful. I would like to thank Dr. Brian Canfield, Alexander Terekhov, and Douglas Warnberg, who have all given me advice and taught me how to use equipment around the lab. I would also like to thank the current and former members of the BEAMS group that have supported me along the way: Dr. Charles Johnson, Dr. Saeed Kamali, Jason Hah, Julie King, Adam Evans, Chad Bond, Anna Bull, and Aleia Williams.

Dr. Richard Lubinsky and Dr. Adrian Howansky from Stony Brook University collaborated with my group on this project, and I would like to thank them for the guidance and knowledge they have given me.

ABSTRACT

Digital radiography (DR) is an important two-dimensional imaging technique in the field of medicine that utilizes x-rays to form a digital image. DR employs a flat panel detector that converts incident x-rays, that have passed through the subject, to an electrical signal, which is used to create a digital image. The conversion from x-rays to electrical signals can be done either directly or indirectly. The direct method involves the x-rays being converted to an electrical signal via an array of semiconductors. The indirect method utilizes scintillators to absorb the x-rays and produce light in the visible spectrum, which is then collected by photodiodes and converted to an electrical signal. One issue that many modern flat panel detectors have is reduced efficiency due to a significant percentage of the incident x-rays passing through the detector without being absorbed. In order to raise the efficiency of these flat panel detectors, rare earth-doped scintillating glass ceramics have been proposed to replace the traditional non-scintillating borosilicate substrates that support the detector electronics. Two series of glass-ceramic scintillators were investigated for this purpose. The first series investigated the potential of calcium fluoride as a scattering center, as well as how the calcium fluoride luminescence behaved when doped with europium. The second series investigated the use of cerium as a sensitizer to improve the scintillating efficiency of terbium. Both series showed that the scattering and luminescent properties of the materials can be controlled. Scintillating glass ceramic materials have the potential to become viable replacements for the un-doped borosilicate substrates that are used in modern flat panel detectors.

TABLE OF CONTENTS

LIST OF FIGURES

INTRODUCTION

Digital Radiography

Digital radiography is a two-dimensional imaging technique that utilizes x-rays to form a digital image. The x-rays are captured after they pass through a patient and are then converted into an electrical signal. This signal can then be turned into a digital image without the need for an intermediate medium like a film or storage phosphor plate. The devices that capture the incoming x-rays and convert them to an electrical signal are called flat panel detectors. Flat panel detectors can use either direct or indirect conversion of the x-rays into an electrical signal [1]. The direct conversion method involves the use of a photoconductor to directly convert the x-ray photons into electrical signals [2]. The indirect method utilizes scintillators to first convert the energy from the x-ray photons into visible light. This visible light is then picked up by a matrix of photodiodes, which convert the light into an electrical signal. A comparison of both conversion methods can be seen in Figure 1 [3]. While the direct conversion method allows for greater spatial resolution than the indirect method, it is only efficient to use for lower energy x-rays [4-10]. In applications where higher energy x-rays are used, the efficiency of the detector drops significantly and the patient will have to be exposed to a higher dosage in order to produce an acceptable image. For this reason, indirect conversion is the most commonly used type of flat panel detector.

A typical indirect conversion flat panel detector consists of 3 main components. The first is the scintillator itself, which is most commonly gadolinium oxysulfide (Gd_2O_2S:Tb) doped with terbium, or cesium iodide (CsI). The scintillator absorbs the incoming x-rays, which excites the electrons in the terbium ions. These electrons return to their ground state by releasing the energy as light, which is picked up by the second component: the photodiodes. The photodiodes take the incoming light and transform it into a voltage. The voltage is then converted by the thin film transistors (TFTs) into an electrical signal that can be used to form an image. This process does not involve the use of any intermediate storage mediums and can be used over a wider array of x-ray energies. There is a loss in resolution with this method when comparing it to direct conversion. This loss is due to light emitted by the scintillator spreading in different directions. The light is not all focused on one point as is the case with x-rays in direct conversion detectors. This spreading of the light increases the point spread function of the detector, which leads to lower image resolution [11-13]. The thickness of the scintillating layer also affects the degree of spreading.

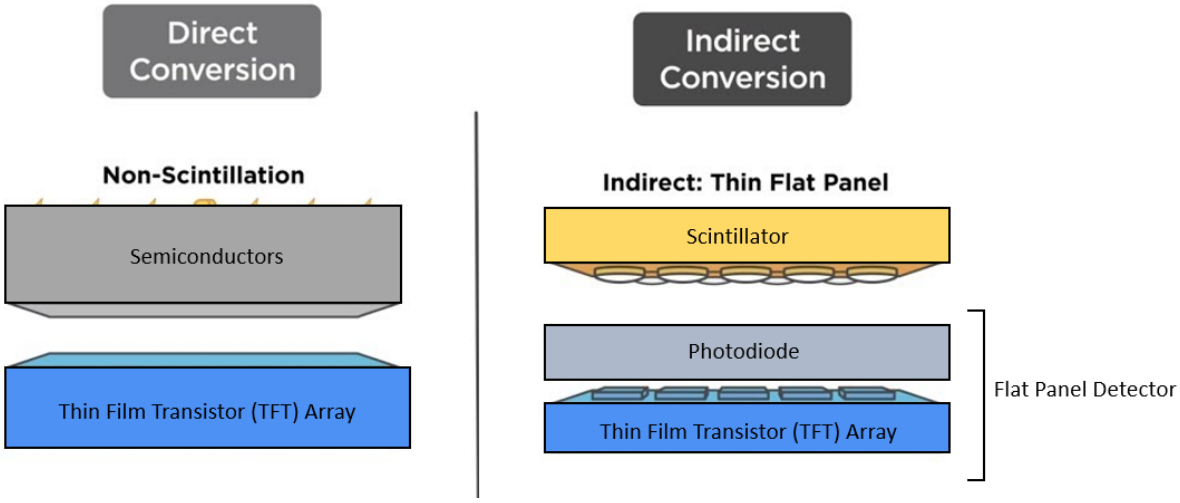

Fig. 1. A comparison of direct and indirect conversion digital radiography detectors. Edited image from [3].

Rare Earth Dopants

The rare earth elements consist of the elements in the lanthanide series of the periodic table, as well as scandium and yttrium. One characteristic of these elements are that they all display trivalent states. These elements have unique properties with regards to their energy levels when compared to other elements. The filled $5s^2$ and $5p^6$ orbitals sit farther out from the nucleus than the 4f orbitals, which causes a shielding effect around the 4f orbitals. This leads to well-defined energy levels, which is not a phenomenon observed in other groups of elements. The emission of light in the rare earth elements is mainly due to 4f-4f emissions and 5d-4f emissions. The use of 5d-4f emissions is usually only seen in Ce^{3+} and Eu^{2+}. The 4f-4f transitions observed in the lanthanide series typically form very sharp emission peaks and the intensity of these emissions is high enough for use in optical devices. Trivalent lanthanide ions are typically used as activators in these optical devices. An example of this is the use of Tb^{3+} in the Gd_2O_2S:Tb scintillators that are commonly used in flat panel detectors [14-15]. The emission of the Tb^{3+} in these scintillators is caused by the $^5D_{3,4}$ to ^7F_J transitions, with the $^5D_4$ to $^7F_5$ transition usually being the dominant one. This transition produces light with a wavelength of 545 nm, which is a wavelength that matches the quantum efficiency curve of the Si photodiodes that are used to convert the light to electrical signals (Figure 2) [16]. Some rare earth elements can also serve as sensitizers, which help transfer energy that is absorbed by the host material to the activators. An example of a common sensitizer is gadolinium [17]. Whether acting as either a sensitizer or an activator, rare earth elements are the primary ions that facilitate the transfer of energy through an intrinsic scintillator.

Oxyhalide Glass Ceramics

Glass ceramics are a type of material that combine the properties of glass and ceramics. They are a mixture of amorphous and crystalline components and can have a wide range of crystallinity depending on their composition and how they are synthesized. Oxyhalide glass ceramics are glass ceramics where the anions consist of oxygen and halides. The size of the crystallites in a glass ceramic can be on the order of nanometers and the appearance of the glass ceramic changes from transparent to opaque as size of the crystals increases. The properties of glass ceramics can be tuned depending on their intended application, but in general they have a high toughness, are very resistant to thermal shock, and experience very little thermal expansion. Glass ceramics can also be chemically and biologically inert, which makes them useful for biomedical applications. The properties of glass ceramics also make them ideal as the host material of a scintillator.

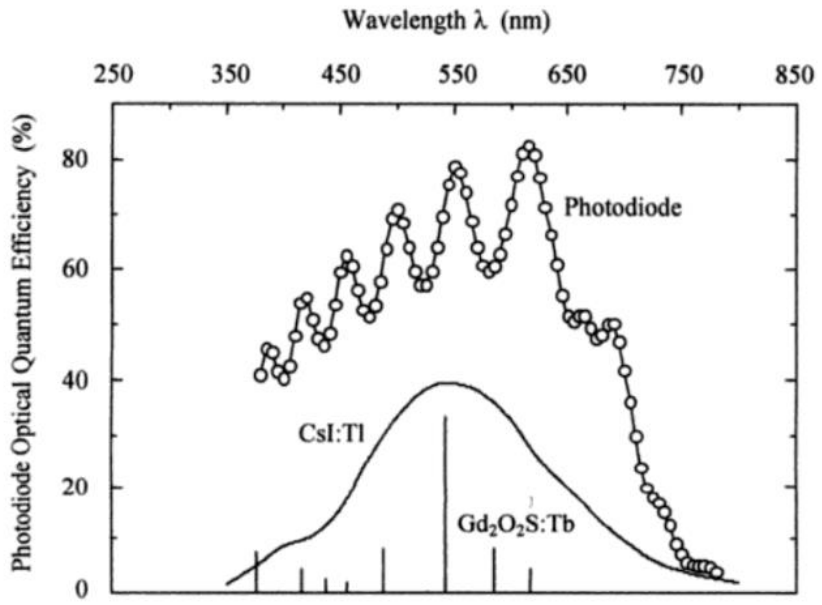

Fig. 2. Quantum efficiency curve for a Si photodiode [16]. Used with permission.

Scintillators for this work are often made of a glass ceramic material, with luminescent dopants embedded in the matrix. Furthermore, they also have properties that make them suitable for acting as the substrate in a digital radiography detector, such as their thermal stability [18]. Changes in the matrix, such as the crystallization, can change how the scintillator interacts with x-rays and emitted photons. Changing the type of material that makes up the crystalline portion of the glass ceramic can alter how the x-rays are absorbed. This can lead to changes in the efficiency of the energy transfer between the incoming photons and the activators in the matrix. Another aspect of halide-containing glass ceramics which makes them favorable for optical applications is that they have a low phonon energy, which lowers the chance for energy to be lost to non-radiative decay [19-21]. The structure of the host material can also change how the photons from the activators are emitted from the material as a whole.

Crystallite particles in the matrix can act as scattering centers for the photons, which alter the path that the emitted photons take to exit the material (Figure 3) [22]. The left image of Figure 3 shows that by introducing scattering centers into the matrix, light trapping is prevented and more of the emitted light is directed towards the side of the scintillator that is facing the detector, thereby increasing the efficiency of the scintillator when compared to pure glass scintillators. With transparent materials, light trapping occurs when emitted photons are reflected internally until they exit the sides of the material [22]. These properties all come together to make glass ceramics very attractive for optical devices, and scintillators in particular.

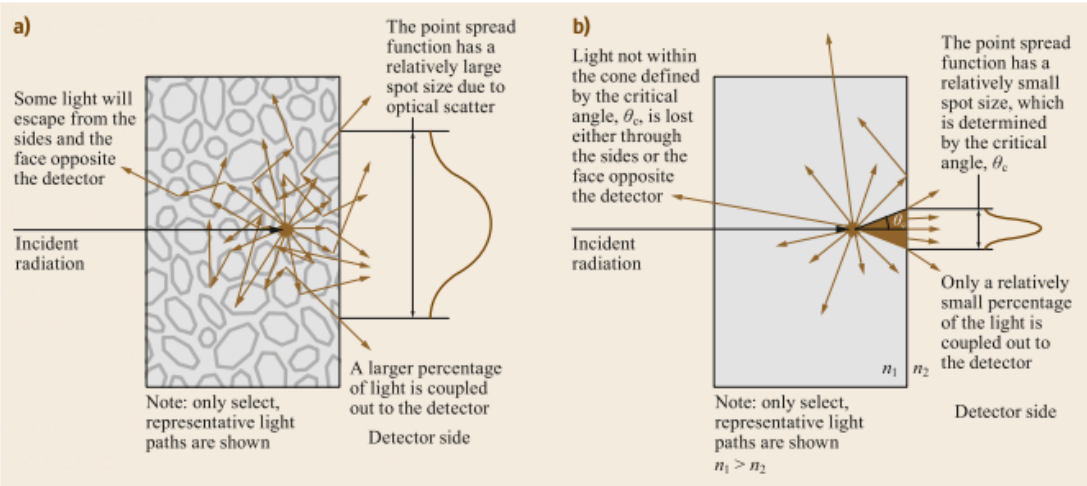

Fig. 3. Comparison of a) a scintillator with scattering centers to b) a transparent scintillator [22]. Used with permission from Springer

CHAPTER I
THE EFFECT OF CALCIUM FLUORIDE CONTENT ON THE LUMINESCENT PROPERTIES OF EUROPIUM-DOPED GLASS CERAMICS

A version of this chapter will be published by Austin Thomas. Austin Thomas was responsible for all research and writing activities with the exception of the x-ray excitation measurements, which were performed by Anthony Lubinsky and Adrian Howansky. Overall guidance was provided by Jacqueline Johnson and Russell L. Leonard.

Abstract

Rare-earth doped oxyhalide glass ceramic substrates can be used to increase the efficiency of x-ray scintillator detectors. Acting as a secondary scintillator behind the flat panel detector, these substrates can capture x-rays that go undetected by the primary scintillator and increase the overall efficiency of the detector. Towards that end, an evaluation of how well the growth of calcium fluoride (CaF_2) crystal precipitates can be controlled, as well as how well the CaF_2 crystals can act as scattering centers in an oxyhalide glass ceramic doped with trivalent europium (Eu^{3+}) was performed. Additionally, the effects of co-doping with Eu^{3+} on the luminescence of the CaF_2 were investigated. A series of four glass ceramic samples containing both CaF_2 and Eu^{3+} were synthesized and heat treated. It was found that the growth of the CaF_2 crystals can be controlled to an acceptable degree. The size of the CaF_2 crystals increased with the amount of CaF_2 in the as-made samples, and further crystal growth was observed after heat treatments. The luminescent intensity of the CaF_2 crystals was found to increase with the amount of crystallinity with no apparent loss of the europium emission intensity. These results show that scintillators made containing both CaF_2 and Eu^{3+} have the potential to act as a replacement material for a flat panel detector substrate.

Introduction

Digital radiography is a type of radiography that involves the direct conversion of x-rays into a digital image without going through a secondary storage medium such as disk or cassette. There are two primary types of digital radiography: direct and indirect conversion. Direct conversion detectors work by directly converting the incoming x-rays into a digital image through the use of semiconductors. Indirect conversion detectors work by first converting the x-rays into visible light, which can then be converted into an image. Indirect conversion digital radiography detectors normally consist of 3 main components. These are the scintillator, electronics, and the substrate. The detector can be described as a ‘sandwich’ with the scintillator on the surface, electronics in the center, and the substrate on the bottom. A scintillator is a type of material that is able to absorb ionizing radiation, such as x-rays, and convert the energy from the absorbed radiation into visible light. This visible light is captured by photodiodes in the flat panel detector, which convert them into a voltage or current. These voltages and

currents can then be converted by the thin film transistors (TFT), which are also a part of the flat panel detector, into an electrical signal that can be processed into a digital image.

One problem that can be found in indirect detectors is a lack of efficiency. A substantial number of x-rays are able to pass through the entire detector without being absorbed. This results in longer exposure times in order to acquire an acceptable image, as well as a higher dosage of radiation for the patients. The substrate that the flat panel detector is attached to is typically made of a non-scintillating borosilicate glass.

This study aims to replace the typical borosilicate glass substrate with a scintillating oxyhalide glass ceramic substrate (Figure 4) [23], which will have the ability to increase the efficiency of the detector as a whole. This glass ceramic substrate will be able to absorb many of the x-rays that are missed by the primary scintillator and emit visible light which will be able to be detected by the photodiodes in the flat panel detector. This will lead to a lower of number of x-rays wasted, thereby increasing the overall efficiency when paired with a bidirectional detector.

While this secondary scintillator must be able to capture x-rays and release light, it still needs to serve as the substrate for the thin-film transistors. Due to this requirement, an oxyhalide glass matrix was retained for the bulk of the material. The properties of oxyhalide glass ceramics make them ideal for use as both a substrate and a scintillator. They are chemically stable, have a high melting temperature, and have a high resistance to thermal shock. These qualities are necessary to serve as the substrate material, as the deposition of the thin-film transistors takes place at around 300°C [24]. Furthermore, they have a low phonon energy, which increases the scintillation efficiency. They can also scatter light depending on how pronounced the crystalline phase is and can have a transparent matrix in order to prevent self-absorption. Too much crystallinity can lead to self-absorption of the emitted light, therefore an ideal scintillator has crystals just large enough to scatter the light and prevent light trapping without being so large as to create a “torturous” path for the photons, which causes significant amounts of self-absorption. Finally, they can have good x-ray attenuation if made with materials that have high x-ray attenuation coefficients.

Calcium fluoride (CaF_2) was chosen as the crystal component for this project due to its many favorable properties. The structure of CaF_2 is well known and it is optically transparent over much of the electromagnetic spectrum from the UV to the NIR [25]. In this study, CaF_2 nanocrystals are precipitated in the glass matrix and act as scattering centers for the emitted light, which will help in preventing light trapping [26]. Furthermore, the CaF_2 itself will also luminesce upon x-ray excitation. While it normally luminesces at around 410 nm, it has been

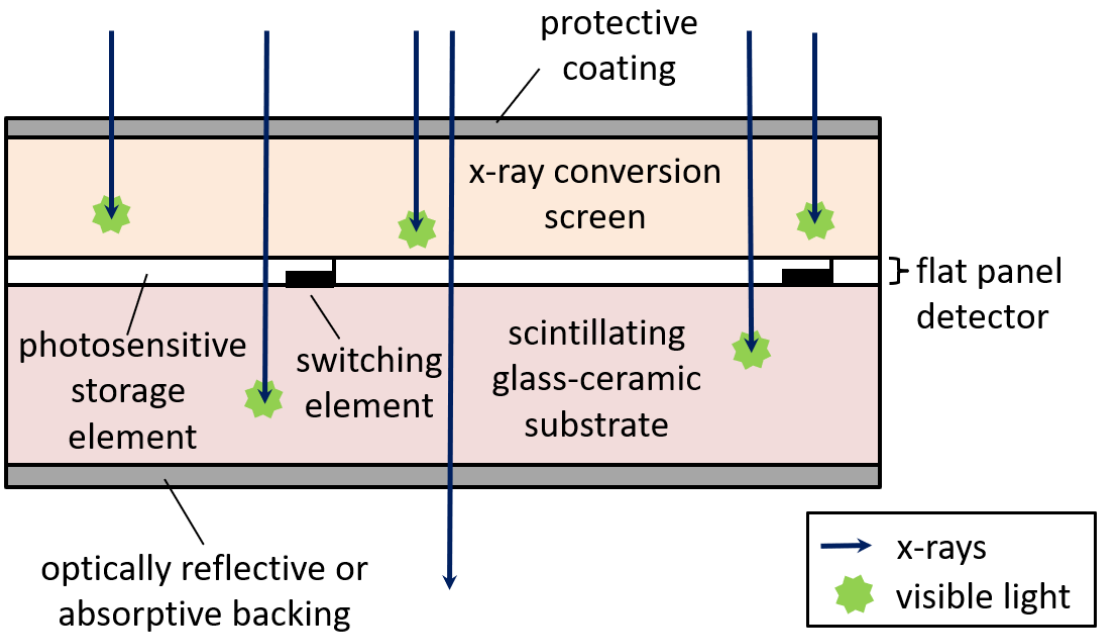

Fig. 4. Visual of a typical x-ray scintillator detector with a scintillating substrate [23]

shown to drastically increase in intensity when doped with Eu, as well as shift to a higher wavelength of around 465 nm [27].

Europium is a well-known luminescent center for scintillator glasses. The primary emission of Eu^{3+} consists of two sharp peaks at 598 nm and 615 nm [28], which matches the quantum efficiency curve of the Si photodiodes reasonably well (Figure 2). It is expected in this study that the crystallization of the CaF_2 will be controllable to a certain degree and that the CaF_2 luminescence will increase with the amount of crystallinity without hindering the luminescence of the Eu^{3+}.

Gadolinium, in the form of gadolinium fluoride (GdF_3), is used in a wide variety of scintillators [29, 30]. It can act as a sensitizer for the primary dopant, in this case Eu^{3+}, and direct the energy from the absorbed x-rays towards the Eu^{3+} ions. Furthermore, gadolinium is a heavy, high Z element, which should help absorb more of the incoming x-rays.

Methods and Materials

Four europium-doped borosilicate glass samples were synthesized according to the following composition:

$$(60\text{-}x)B_2O_3 + 5SiO_2 + 10GdF_3 + 2Eu_2O_3 + 23Li_2O + xCaF_2$$

with x being 20, 22, 25, and 30. These samples were synthesized inside a glovebox (MBRAUN Labmaster SP), which contained an argon atmosphere in order to prevent the intrusion of any moisture or oxygen into the sample during synthesis. The precursor powders for each sample were first weighed and dried as needed in a programmable tube furnace (MTI Corporation OTF-1200X) at 400°C. All of the powders were then mixed together in a platinum crucible and dried again in the furnace to confirm the absence of moisture. The mixture was weighed one last time to determine any mass loss from the drying then returned to the furnace. The mixture was heated up to 1000°C over the course of 3 hours, at which point it was poured into a brass mold. The mold was preheated to 400°C by cartridge heaters controlled by a proportional-integral-derivative system in order to prevent thermal shock in the samples. The mold was cooled to room temperature over the course of 4 hours.

Differential scanning calorimetry (DSC) was performed using a Netzsch DSC 200F3. The samples were heated from 300°C to 590°C at a rate of 10K/min using a nitrogen purge gas.

After synthesis, the samples were heat treated in a Blue M ULTRA-TEMP Convection Oven. The samples were heat treated at temperatures corresponding to thermal events shown in the DSC results. Along these lines, the 20% CaF_2,

25% CaF_2, and 30% CaF_2 samples were heat treated at 470°C for 10 minutes, and the 20% CaF_2, 22% CaF_2, and 25% CaF_2 samples were heat treated at 525°C for 10 minutes. The goal of these heat treatments is to precipitate CaF_2 crystals in the sample, as well as understand the phase transformation seen in the DSC results.

The samples were analyzed using X-ray diffraction in order to confirm the presence of CaF_2 crystals in the matrices of the samples, as well as identify any other phases that may be present. This was performed on a Philips X'Pert MRD X-ray Diffractometer (PANalytical Inc.) with a Cu anode X-ray source. The scan range was 20° to 80° 2θ. The step size was 0.05° and the time per step was 35 seconds.

A QM-3-PH phosphorescence/ fluorescence spectrofluorometer (Photon Technology International Inc.) was used to measure the emission and excitation spectra of the samples. The system utilized an R1527P Photomultiplier tube and a Type L4633 Xenon Flash Lamp (Hamamtsu Photonics K.K.). The data analysis was performed using Felix32 software. A measurement of the excitation spectrum was taken for all samples for an emission of 615 nm, which is the primary peak for an Eu^{3+} emission. Measurements of the emission spectra for the samples were taken at the major peak that emerged in the excitation spectra of all the samples, which was 395 nm. For all samples, the step size was 1 nm, the integration time was 1 ms, and 3 scans were performed per measurement.

Spectrophotometry was performed using a Gentech Scientific TU-1901 UV-VIS spectrophotometer in order to quantify the transparency of the samples. Spectrophotometry was only performed on the samples that appeared to be transparent or translucent, as any opaque samples would not produce a spectrum.

Results and Discussion

Differential Scanning Calorimetry

DSC analysis was performed on each sample after synthesis (Figure 5). For all four samples, the glass transition begins at around 390°C. Both the 25% and 22% CaF_2 samples experience large thermal events, which are indicated by the tallest peaks of the two spectra. These events, at 470°C for the 25% sample and at 525°C for the 22% sample, are most likely the crystallization of the samples. These two peaks are the reason that 470°C and 525°C were chosen as the temperatures for the heat treatments. The 22% CaF_2 sample was not heat treated at 470°C because it is unlikely that any crystallization would have occurred according to the DSC results. The 25% CaF_2 was also heat treated at 525°C due to the secondary peak that occurs there in its spectrum. As the 30%

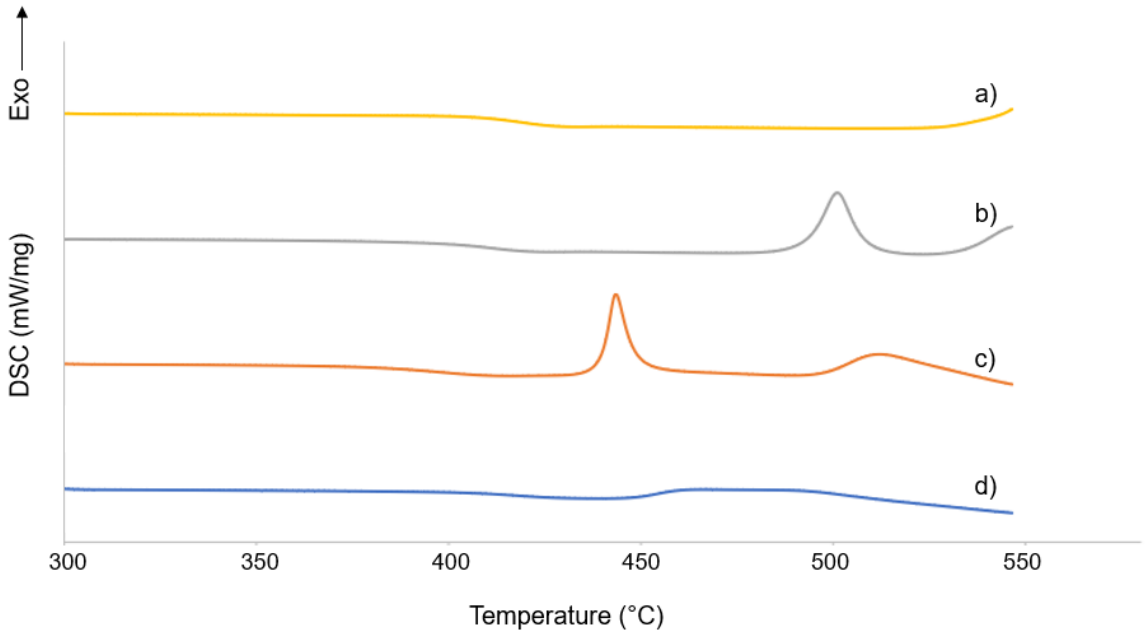

Fig. 5. DSC analysis of the as-made samples. a) 20% CaF_2, b) 22% CaF_2, c) 25% CaF_2, and d) 30% CaF_2

CaF_2 sample had already crystallized before the DSC occurred, it does not have a crystallization peak. The 30% CaF_2 sample was instead only heat treated at 470°C as that is where the beginning of the broad peak in its spectrum is located. While it is somewhat unclear what event takes place at this peak, it is possible that it represents a phase change of some kind. The 20% CaF_2 sample was heat treated at both 470°C and 525°C. This is because according to the DSC results, it does not have any thermal events other than the glass transition takes place within the limits of the DSC instrument. There is the beginning of a peak near the end of the spectrum, which is likely the point that crystallization.

Visual Inspection

After synthesis, the samples were visually inspected (Figure 6). The 30% CaF_2 sample appears completely opaque, while the other three are mostly transparent. Some crystallinity can be seen in the 22% and 25% CaF_2 samples, with the top of the samples crystallizing as well as small crystallites being scattered throughout the matrix. The crystallinity at the top of the two samples can be attributed to that face being exposed to air, while the other faces were in contact with the heated mold. This caused the exposed face to cool down at a slower rate and subsequently crystallize. The size of the small crystallites is tied to the CaF_2 content of the sample, as the crystallites in the 25% CaF_2 sample are visibly larger than those in the 22% CaF_2 sample.

After heat treatment, the samples were again inspected visually (Figure 7). As seen in the top row of Fig. 3, the 30% CaF_2 sample has not visually changed, as it was crystallized to begin with. The 25% CaF_2 sample was crystallized after heat treatment at 470°C, while the 20% CaF_2 sample has not crystallized at all. In the bottom row, it can be seen that both the 25% and 22% CaF_2 samples are crystallized after being heat treated at 525°C, as they are both opaque. The 20% CaF_2 sample has partially crystallized and now appears translucent.

The samples under exposure to a 365 nm UV lamp can be seen in Figure 8. As can be seen in the top row of Fig. 4, the 20% and 22% CaF_2 samples exhibit only the orange-colored emission that is characteristic of Eu^{3+}. The 25% CaF_2 sample shows mostly orange emission throughout the matrix, but the crystalline portions of the sample are bright purple. Calcium fluoride traditionally emits at 410nm, which would appear as violet luminescence. The most likely cause of this light purple emission is CaF_2 luminescence that has been shifted to a slightly higher wavelength. After heat treatment at 470°C, the 30% and 25% CaF_2 samples both exhibit the light purple emission, while the

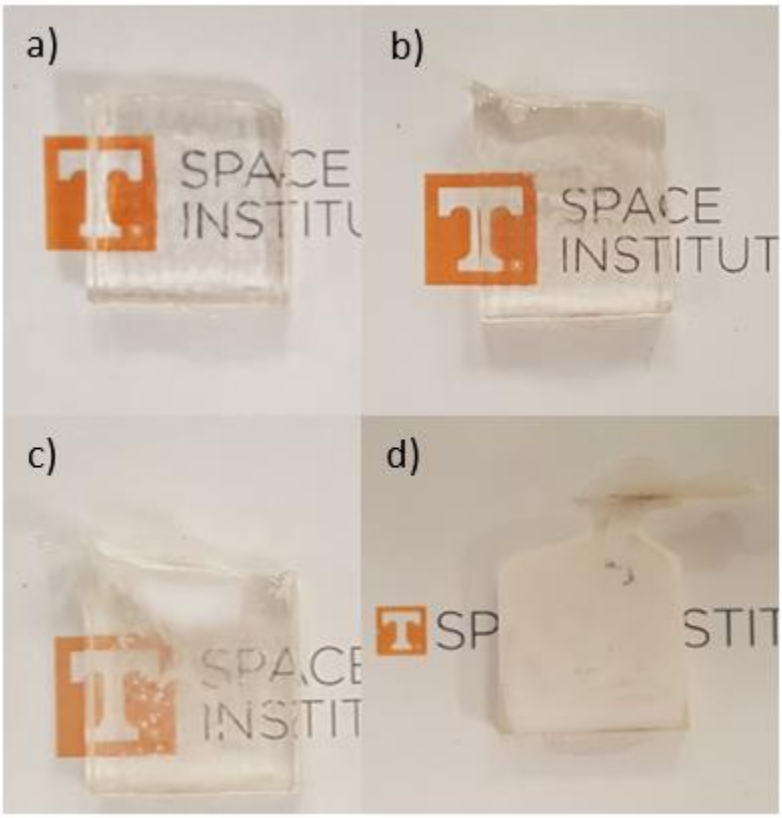

Fig. 6. Visual comparison of the samples post synthesis.
a) 20% CaF_2, b) 22% CaF_2, c) 25% CaF_2, and d) 30% CaF_2

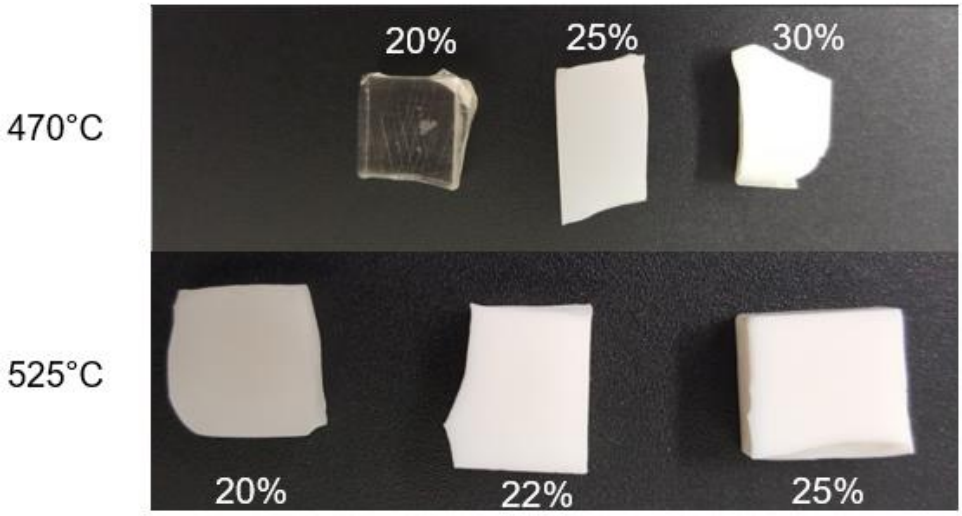

Fig. 7. Visual comparison of samples heat treated at 470°C (Top) and 525°C (Bottom)

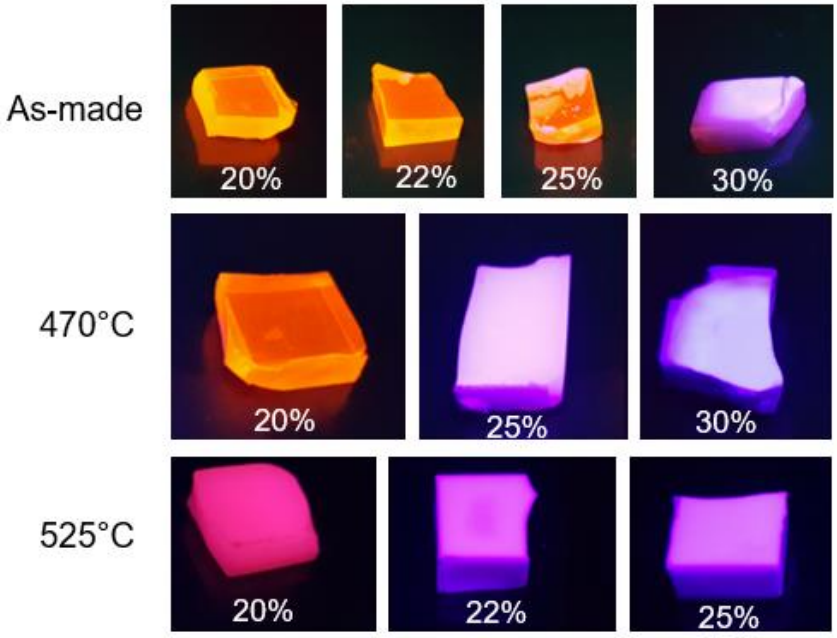

Fig. 8. Visual comparison of synthesized samples under 365 nm excitation of the As-made samples (Top), samples heat treated at 470°C (Middle), and samples heat treated at 525°C (Bottom)

20% CaF_2 sample has yet to crystallize and still shows the orange emission. In the bottom row, the 25% and 30% CaF_2 samples show the same purple emission. The 20% CaF_2 sample shows a different shade of the purple emission, which may be due a lesser amount of CaF_2 emission or some reflection from the UV lamp.

X-Ray Diffraction

XRD analysis of the samples was performed in order to confirm the presence of CaF_2 crystals in the matrix. Looking at Figure 9, it can be seen that CaF_2 crystals were successfully precipitated. The black bars near the bottom represent the characteristic peaks according to ICSD card number 82707 (CaF_2). These peaks are quite clear in the 30% CaF_2 sample, as well as in the 25% and 22% samples after they were heat treated. The spectra for several of the samples is seen to be shifted slightly from the characteristic CaF_2 peaks, but this can be attributed to a Z-error in the sample placement. They can also just barely be seen in the 20% sample after heat treatment at 525°C. There is an unidentified second phase that appears in several of the samples. These peaks are located roughly at 38, 45, and 66 degrees two theta. They show up in the 30%, 25% and 22% CaF_2 samples after heat treatment and in the 20% CaF_2 sample only after heat treatment at 470°C. This phase is not present in the 25% and 22% CaF_2 samples before they are heat treated, even though they have some partial crystallization. Furthermore, they disappear from the 20% CaF_2 sample after heat treatment at 525°C, even though they are present after heat treatment at 470°C. This phase has not yet been identified. Another point of interest is a possible third phase that is unknown in the as-made 30% CaF_2 sample. The two peaks, situated around 36 and 43 degrees two theta, are shifted too far from the peaks of the other unknown phase to be attributed to error, which would suggest that they belong to a separate phase.

Phosphorimetry

The results for the as-made samples can be seen in Figure 10. All four of the as-made samples exhibit the classic Eu^{3+} peaks at 598 nm and 615 nm. Only the 30% CaF_2 sample exhibits any emission around 450 nm, which is indicative of CaF_2 emission as noted earlier. Due to the 30% CaF_2 sample showing both CaF_2 and Eu^{3+} emissions, the author hypothesized that the purple emissions seen with many of the samples is actually a combination of the CaF_2 and Eu^{3+} luminescence. The results for each composition can be seen in Figure 11, 12, 13, and 14. In the 20% CaF_2 sample, no CaF_2 emission can be seen either before or after heat treatment at both 470°C and 525°C. This is at odds with the visual examination of the sample back in Figure 8, where the emission does not appear to be that of Eu^{3+}.

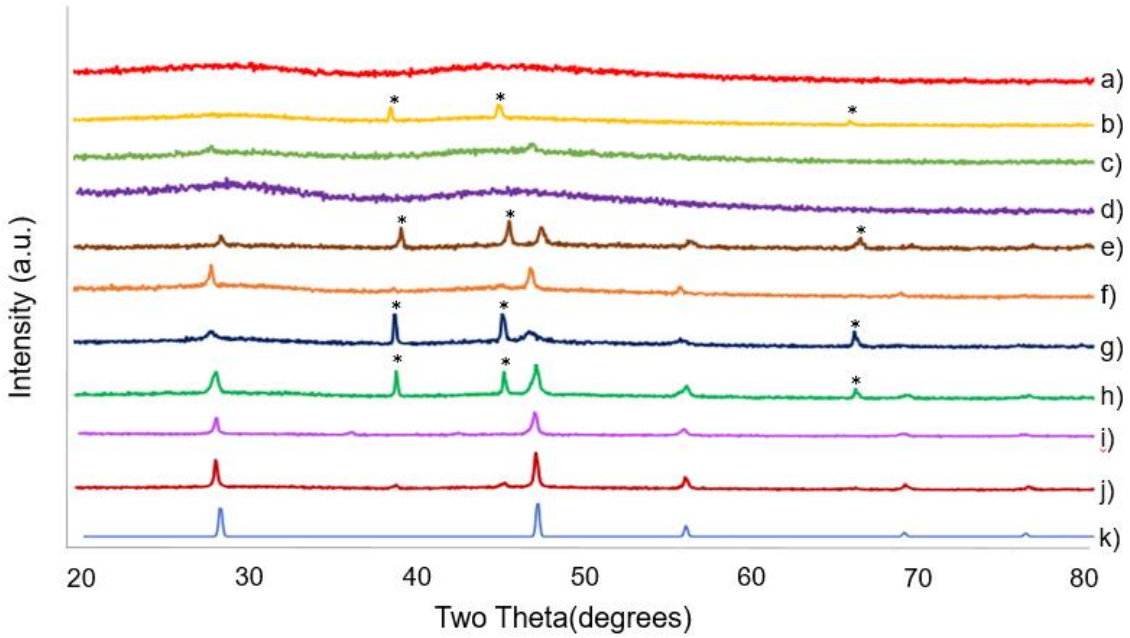

Fig. 9. XRD Spectra of all samples. a) as-made 20% CaF_2, b) 20% CaF_2 heat treated at 470°C, c) 20% CaF_2 heat treated at 525°C, d) as-made 22% CaF_2, e) 22% CaF_2 heat treated at 525°C, f) as-made 25% CaF_2, g) 25% CaF_2 heat treated at 470°C, h) 25% CaF_2 heat treated at 525°C, i) as-made 30% CaF_2, j) 30% CaF_2 heat treated at 470°C, and k) ICSD col. 82707 (CaF_2). "*" Denotes an unknown secondary phase

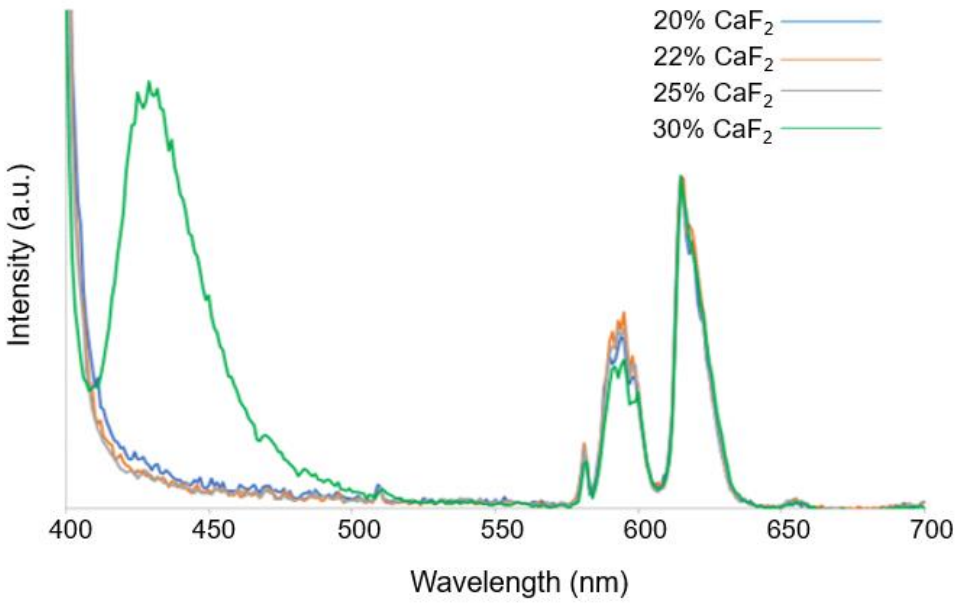

Fig 10. Emission spectra of as-made samples at 395 nm excitation normalized to the peak at 615 nm

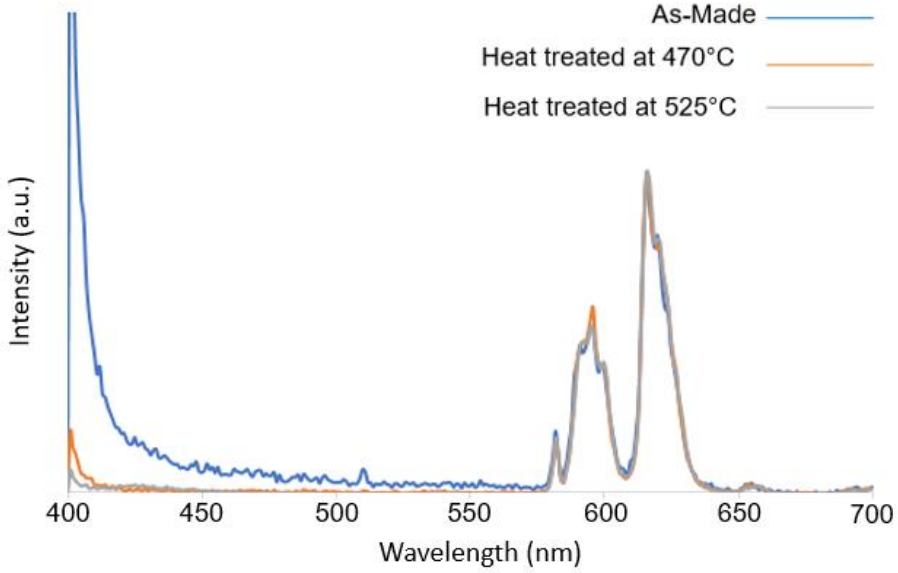

Fig. 11. Emission spectra of the 20% CaF_2 samples at 395 nm excitation normalized to the peak at 615 nm

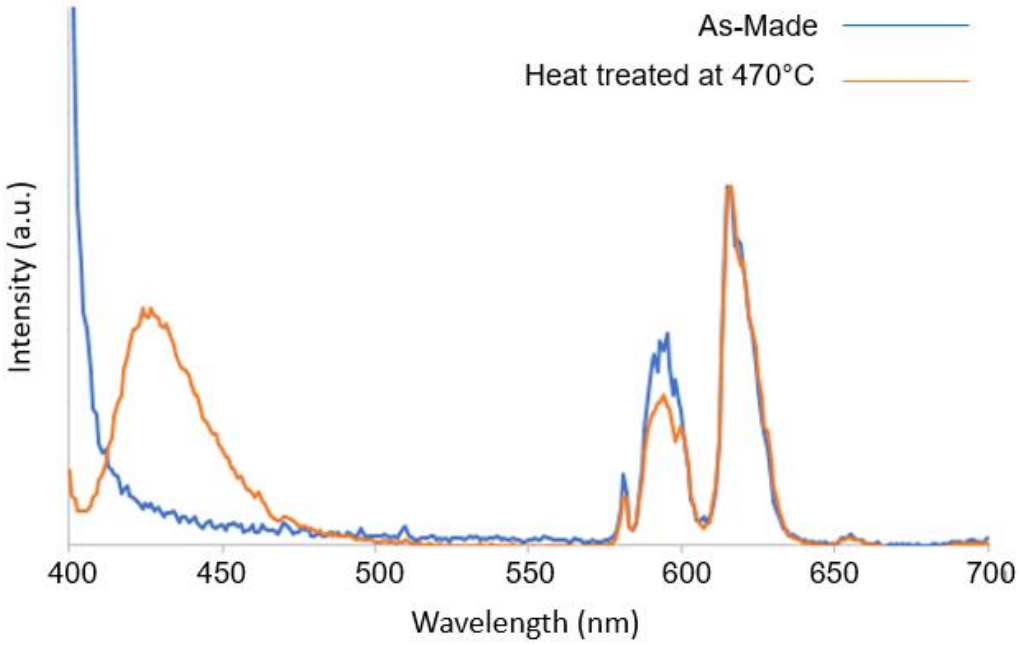

Fig. 12. Emission spectra of the 22% CaF_2 samples at 395 nm excitation normalized to the peak at 615 nm

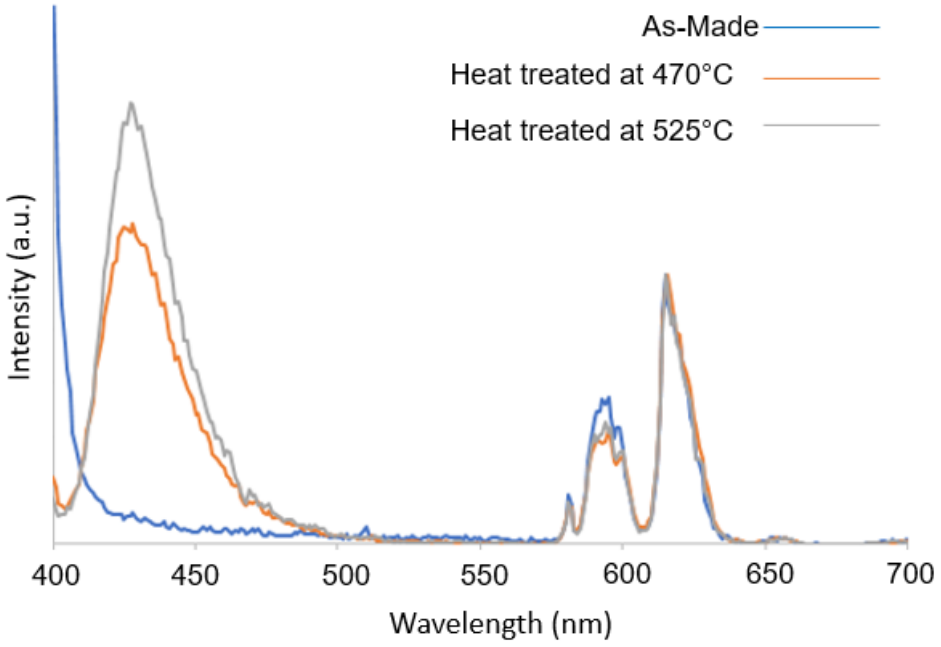

Fig. 13. Emission spectra of the 25% CaF_2 samples at 395 nm excitation normalized to the peak at 615 nm

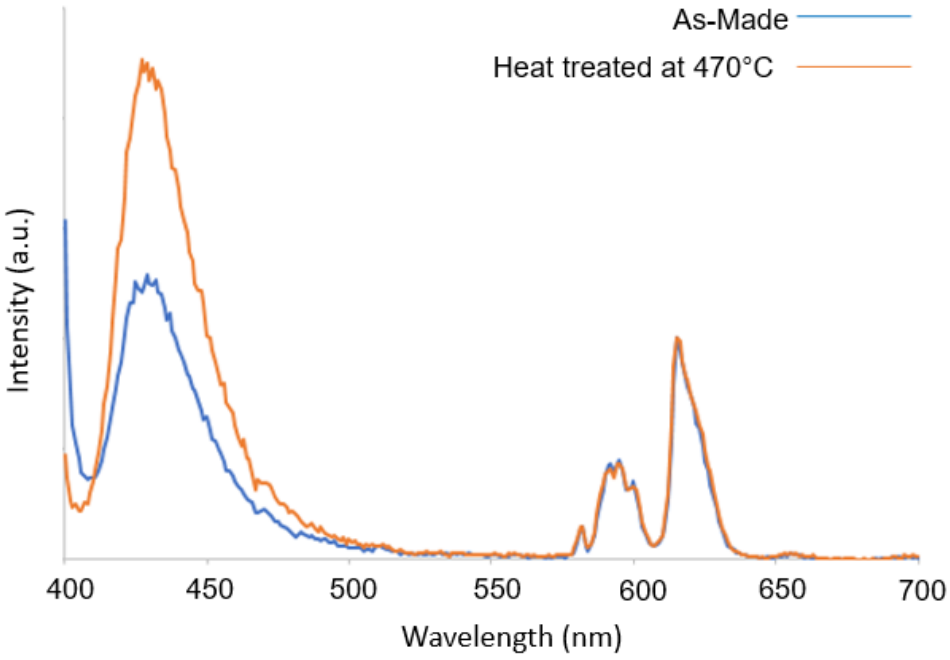

Fig. 14. Emission spectra of the 30% CaF_2 samples at 395 nm excitation normalized to the peak at 615 nm

For the 22% CaF_2 sample, CaF_2 emission can be seen after heat treatment at 525°C. This is also viewed in the 25% CaF_2 sample, where the CaF_2 emission can be seen after heat treatment at both 470°C and 525°C, and the CaF_2 emission is stronger after heat treating at a higher temperature. In both the 22% and 25% CaF_2 samples, there is a slight decrease in the relative intensity of the 598 nm peak after heat treatment. This could possibly be attributed to scattering caused by CaF_2 crystals that form after heat treatment [31, 32]. Another possibility is that the CaF_2 could be competing with Eu^{3+} for the energy that would normally be emitted as the 598 nm emissions. Finally, a CaF_2 emission can be seen in the 30% CaF_2 sample before and after heat treatment, due to the sample crystallizing during synthesis. The CaF_2 emission does increase after the heat treatment, which would suggest that not all of the CaF_2 in the matrix had crystallized prior to the heat treatment.

These results show that the precipitation of the CaF_2 crystals in the matrix have a significant effect on the luminescent properties of the samples. Once the CaF_2 is precipitated, a strong CaF_2 emission signal can be detected. Furthermore, there is no significant change in the Eu^{3+} emission spectrum as a result of the CaF_2.

Spectrophotometry

Spectrophotometry was performed on the as-made samples, as well as on the samples after heat treatment at 470°C and 525°C (Figure 15). The transmittance of the as-made samples decreases with increasing CaF_2 content. This decrease in the as-made samples is due to the increased amount of crystallization, which leads to more light being scattered. The absorption peaks that can be seen in all of the as-made samples are some of the characteristic absorption peaks of Eu^{3+} [33]. The results for the 20% CaF_2 samples can be seen in Figure 9. When looking at just the 20% CaF_2 sample, it can be seen that the transmission drops slightly after the heat treatment at 470°C, which coincides with how it looks visibly. Similarly, the transmittance is almost zero across the entire range of wavelengths after the heat treatment at 525°C, where the sample appears opaque. As expected, the precipitation of CaF_2 crystals results in a drop in transmission.

Conclusions

The amount of scattering in the as-made samples is found to be closely tied to the amount of CaF_2 used during synthesis. The as-made sample containing 20% CaF_2 did not appear to crystallize at all, while the sample slightly crystallized after heat treatment at 525°C. Partial crystallization was observed

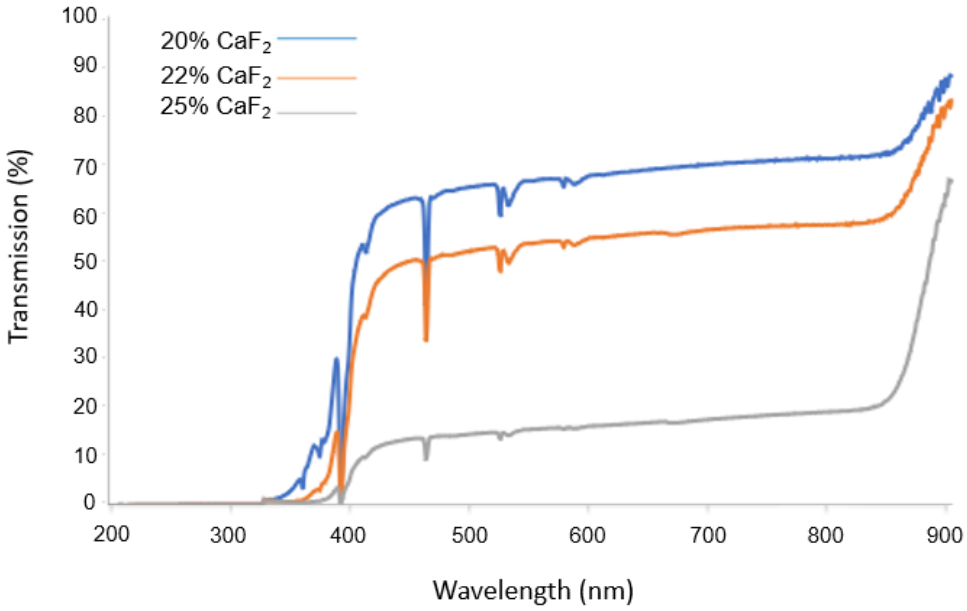

Fig 15. Transmission spectra of the as-made samples

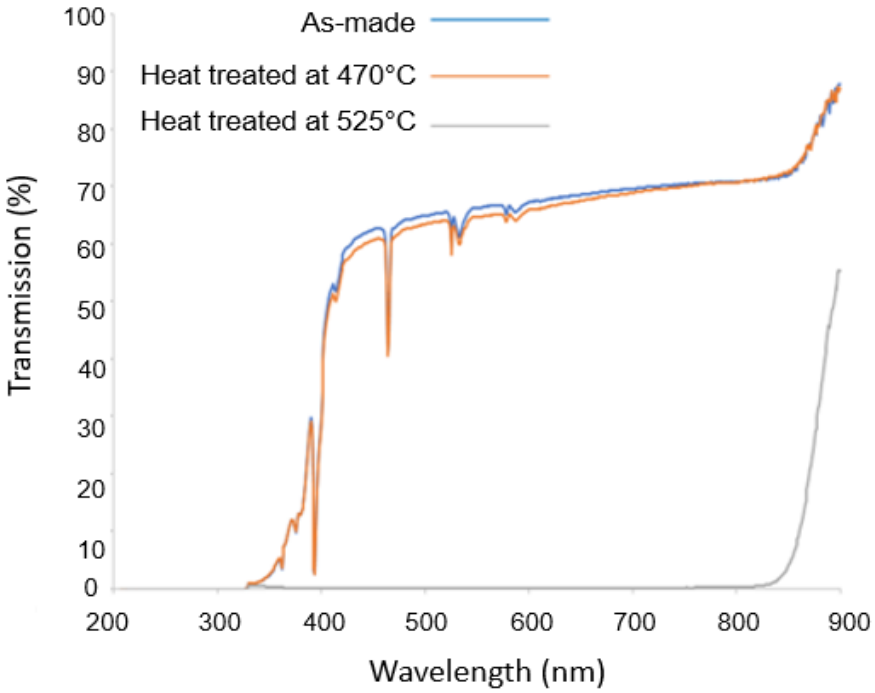

Fig. 16. Transmission spectra of the 20% CaF_2 samples

in the 22% and 25% CaF_2 samples upon synthesis and they both crystallized after heat treatments at 470°C and 525°C. Furthermore, the degree of crystallinity was greater in the 25% CaF_2 as-made sample when compared to the 22% CaF_2 as-made sample as could be seen in the visual inspection. Finally, the 30% CaF_2 appeared fully opaque after synthesis, which would indicate almost complete crystallization. The presence of CaF_2 crystals is confirmed by the XRD data, which shows the characteristic peaks of CaF_2 crystals in all of the samples after heat treatment, as well as in the 30% CaF_2 sample beforehand. A purple luminescence was observed in the crystallized samples under UV exposure, which is likely a combination of CaF_2 and Eu^{3+} emissions. This is further supported by the phosphorimetry results, which show the presence of CaF_2 emission in the crystalline samples, as well as an increase in the CaF_2 emission when the samples were heat treated at higher temperatures. The spectrophotometry results show a loss in transmission with increased CaF_2 content, likely due to additional precipitation and growth of CaF_2 crystals. Further research is needed in order to fully understand the mechanisms of the crystal growth in this series, as evidenced by the two unknown phases that appear in several of the XRD spectra. The results seen in this study show that the crystallization of CaF_2 crystals in an oxyhalide glass matrix can be controlled, which means that the amount of scattering can be controlled. This can allow for fine tuning of the crystallization in order to reach a degree of crystallinity that is optimized for performing as a scintillator in a digital radiography detector.

Further work can be done on these samples in order to investigate the emission properties of these scintillators under x-ray excitation. The output of these materials under x-ray excitation could vary widely from what can be seen under UV excitation [23].

CHAPTER II
THE EFFECTS OF CERIUM CO-DOPING ON THE LUMINESCENT PROPERTIES OF TERBIUM IN OXYHALIDE GLASS CERAMICS

A version of this chapter will be published by Austin Thomas. Austin Thomas was responsible for all research and writing activities with the exception of the x-ray excitation measurements, which were performed by Anthony Lubinsky and Adrian Howansky. Overall guidance was provided by Jacqueline Johnson and Russell L. Leonard.

Abstract

Indirect digital radiography detectors work by absorbing the incoming x-rays with a scintillator. This scintillator emits visible light, which is picked up by the flat panel detector, and uses it to make a digital image. One problem that indirect detectors experience is a lack of efficiency due to x-rays passing through the detector without being absorbed. In this study, a series of scintillators were made with the purpose of replacing the electronics substrate in order to increase the efficiency of the detector by absorbing the x-rays that aren't absorbed by the rest of the detector. In this series, the effect of cerium fluoride as a sensitizer for terbium ions in an oxyhalide glass ceramic matrix was investigated. By co-doping both cerium and gadolinium with the terbium, the transfer of energy to the terbium ions should become more efficient. A series of samples was made with varying amounts of cerium fluoride added. The amount of light detected was found to decrease with both the amount of cerium fluoride added and the precipitation of calcium fluoride crystals.

Introduction

One type of radiography that is commonly used in the medical field is digital radiography. Digital radiography is a technique that involves the direct conversion of x-rays into a digital image without the use of a storage medium. There are two types of digital radiography detectors: direct conversion and indirect conversion. Direct conversion detectors use semiconductors to directly convert incoming x-rays into an electrical signal that can be used to form a digital image. Indirect conversion detectors first convert the x-rays into visible light through the use of a scintillator, which is a type of material that can absorb ionizing radiation and emit visible or near-visible light. Two scintillators that are widely used in digital radiography are gadolinium oxysulfide (Gd_2O_2S: Tb) doped with terbium, and cesium iodide (CsI). The photons emitted by the scintillator are picked up by photodiodes that reside in the flat panel detector and converted into a voltage. The thin film transistors that also reside in the flat panel detector then use those voltages to create an electrical signal that can be turned into a digital image. In a typical detector, all of these components rest on top of a non-scintillating substrate, usually a borosilicate glass. One drawback of indirect conversion detectors is a reduced efficiency. In these detectors, a significant number of

x-rays pass through the detector without being absorbed, which leads to increased dosages in order to get an acceptable image. In this study, oxyhalide glass ceramic scintillators are studied with the intention of replacing the regular substrates in the detectors (Figure 4). By replacing the substrate with a second scintillator, any x-rays that are not absorbed by the rest of the detector can still be absorbed by this scintillating substrate, which can in turn emit visible light that can be picked up by the photodiodes. This would increase the overall efficiency when paired with a bidirectional detector.

Oxyhalide glass ceramics were chosen as the material for these scintillating substrates due to their many favorable properties. They are chemically and thermally stable, which is important due to the flat panel detector typically being deposited on the substrate at 300°C [24]. Glass ceramics can also be made with materials that have high x-ray attenuation coefficients.

One important aspect of glass ceramics is the crystalline component, which act as scattering centers for the emitted light. These scattering centers reduce the mean free path of the emitted photons, which helps to prevent light trapping, allowing more of the emitted photons to exit the scintillator at the surface closest to the detector [26]. If the crystals grow to be too large in size or number, there can be an increase in self-absorption of the emitted light due to excessive scattering.

Terbium is a commonly used dopant for luminescent applications. It has a very strong emission intensity at a wavelength of 545nm, which matches the quantum efficiency curve of the Si photodiodes very well [2]. It is for these reasons that terbium is often used as the primary dopant in the non-intrinsic scintillators that are used in indirect detectors.

Both gadolinium and cerium are used as co-dopants in this series, where they will act as sensitizers for the terbium ions. The hypothesized energy transfer mechanisms in this series involve the transfer of energy from the cerium ions to the gadolinium ions, and from the gadolinium ions to the terbium ions [21]. The author posits that the addition of cerium will enhance the luminescent efficiency of the scintillator by improving the transfer of energy to the terbium ions.

Materials and Methods

A series of five terbium-doped samples were synthesized according to the following formula:

$$(36\text{-}x)B_2O_3 + 5SiO_2 + 10GdF_3 + 6TbF_3 + 23Li_2O + 20CaF_2 + xCeF_3$$

where x is 0, 2, 4, 6, and 8. These samples were made inside a glovebox (MBRAUN Labmaster SP). In order to prevent any moisture or oxygen from interacting with the sample, the glovebox was filled with an inert argon atmosphere. The precursor powders for each sample were weighed and mixed inside a platinum crucible. The powders were dried inside a programmable tube furnace (MTI Corporation OTF-1200X) at 400°C as needed in order to remove any moisture. The entire mixture was dried again afterwards in order to confirm a lack of moisture and subsequently returned to the furnace. The mixture was then heated up to 1000°C over the course of 3 hours, after which it was poured into a brass mold. The mold was preheated to 400°C by cartridge heaters controlled by a proportional-integral-derivative system in order to prevent thermal shock in the samples. The mold was cooled to room temperature over the course of 4 hours.

Differential scanning calorimetry (DSC) was performed using a Netzsch DSC 200F3. The samples were heated from 300°C to 590°C at a rate of 10K/min using nitrogen purge gas.

After synthesis, a portion of the samples were heat treated in a Blue M ULTRA-TEMP Convection Oven. The samples were heat treated according to thermal events shown in the DSC results. Along these lines, the 0% CeF_3, sample was heat treated at 453°C, 455°C, and 465°C. The 2% CeF_3 sample was heat treated at 430°C, 432°C, and 435°C. The 4% CeF_3 sample was heat treated at 412°C and 415°C. The 6% CeF_3 was heat treated at 387°C, 390°C, and 395°C. The 8% CeF_3 sample was heat treated at 400°C.

The samples were analyzed using x-ray diffraction in order to confirm the presence of CaF_2 crystals in the samples as well as identify any other phases that may exist. This was performed on a Rigaku Smart Lab X-ray Diffractometer with a Cu anode X-ray source. The scan range was 10° to 80° 2θ. The step size was 0.1°, and the time per step was 4 seconds.

A QM-3-PH phosphorescence/ fluorescence spectrofluorometer (Photon Technology International Inc.) was used to measure the emission spectra of the samples. The system utilized an R1527P Photomultiplier tube and a Type L4633 Xenon Flash Lamp (Hamamtsu Photonics K.K.). Data analysis was performed using the Felix32 software. Measurements of the emission spectra for the samples were taken 395 nm. For all samples, the step size was 1 nm, the integration time was 1 ms, and 3 scans were averaged per measurement.

Spectrophotometry was performed using a Gentech Scientific TU-1901 UV-VIS spectrophotometer in order to evaluate the transparency of the samples. Spectrophotometry was only performed on the samples that appeared to be transparent or translucent. The 8% CeF_3 samples, being opaque, were not measured.

The x-ray scintillation output was measured using a modified x-ray flat panel detector. The housing of a commercial indirect flat panel detector (AXS-2430FDi, Analogic Canada Corporation) was modified in order for the scintillator samples to be pressed directly onto the TGT and photodiode layers [34]. The apparatus could be rotated in order to measure both “front irradiated” and “back irradiated” excitation. In this case, back irradiated signal intensity was measured in order to more accurately assess these materials as scintillating substrates, where they would be sitting behind the flat panel detector [35-36]

Results and Discussion

Differential Scanning Calorimetry

The DSC results can be seen in Figure 17. The glass transition temperature of the samples occurs at around 375°C. The tall peaks indicate the crystallization of the CaF_2 in the matrix and shift down to lower temperatures as the amount of CeF_3 in the samples is increased. This is most likely due to the additional CeF_3 providing more fluorine ions for the calcium ions to interact with in order to form the crystallites. Additional peaks can be seen in the spectra of the 0-4% CeF_3 samples, which is most likely the peak of crystallization for a secondary crystal phase.

Visual Inspection

The five as-made samples, as well as the heat-treated samples, can be seen in Figure 18a. The coloration of the samples gradually changes from clear to yellow, and then to a darker brown as the amount of CeF_3 in the sample is increased. The 8% CeF_3 sample is an extremely dark brown and has also crystallized on the inside. The heat-treated samples appear to be more opaque than the as-made samples, which indicate the precipitation and growth of crystals. The opacity of the samples was further found to increase with the heat treatment temperature. Only the 8% CeF_3 appears to be mostly crystallized as-made, as it doesn’t appear different after being heat treated. The samples can also be seen under UV excitation in Figure 18b. The green luminescence of terbium emissions can be observed in the samples and the intensity of the emission decreases as the amount of CeF_3 in the samples is increased. This result disagrees with the hypothesis that Ce^{3+} should improve efficiency.

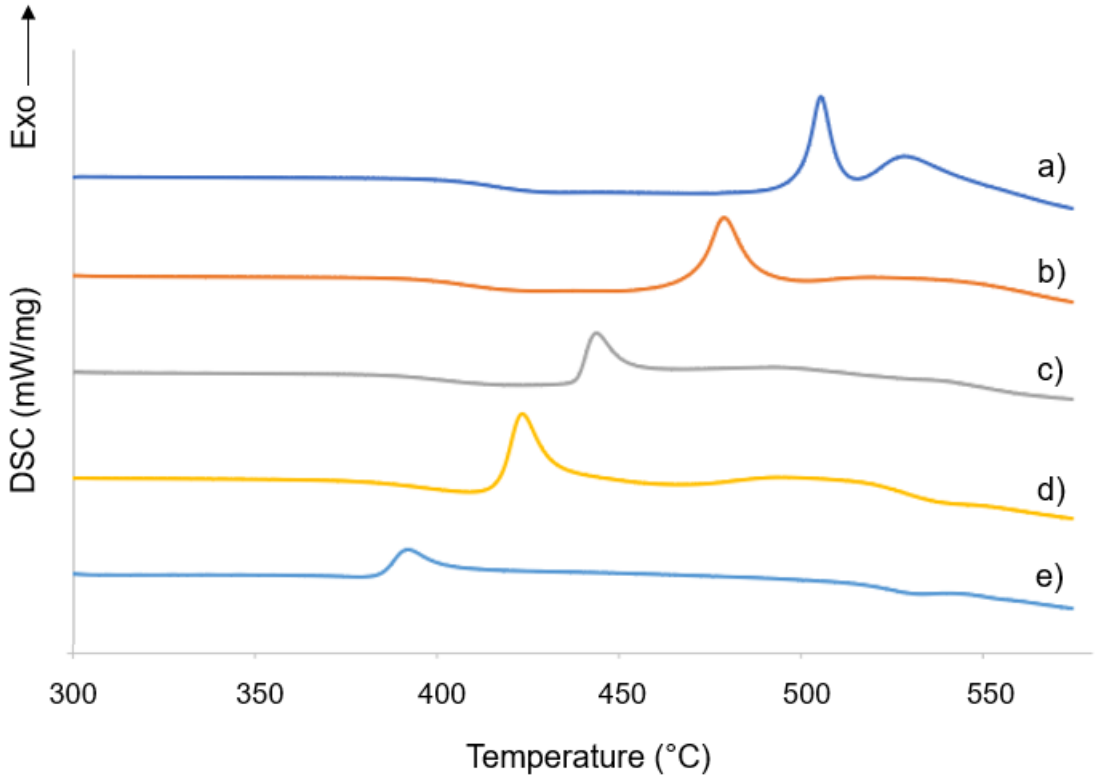

Fig 17. Differential scanning calorimetry results for the as-made samples. a) 0% CeF_3, b) 2% CeF_3, c) 4% CeF_3, d) 6% CeF_3, and 3) 8% CeF_3

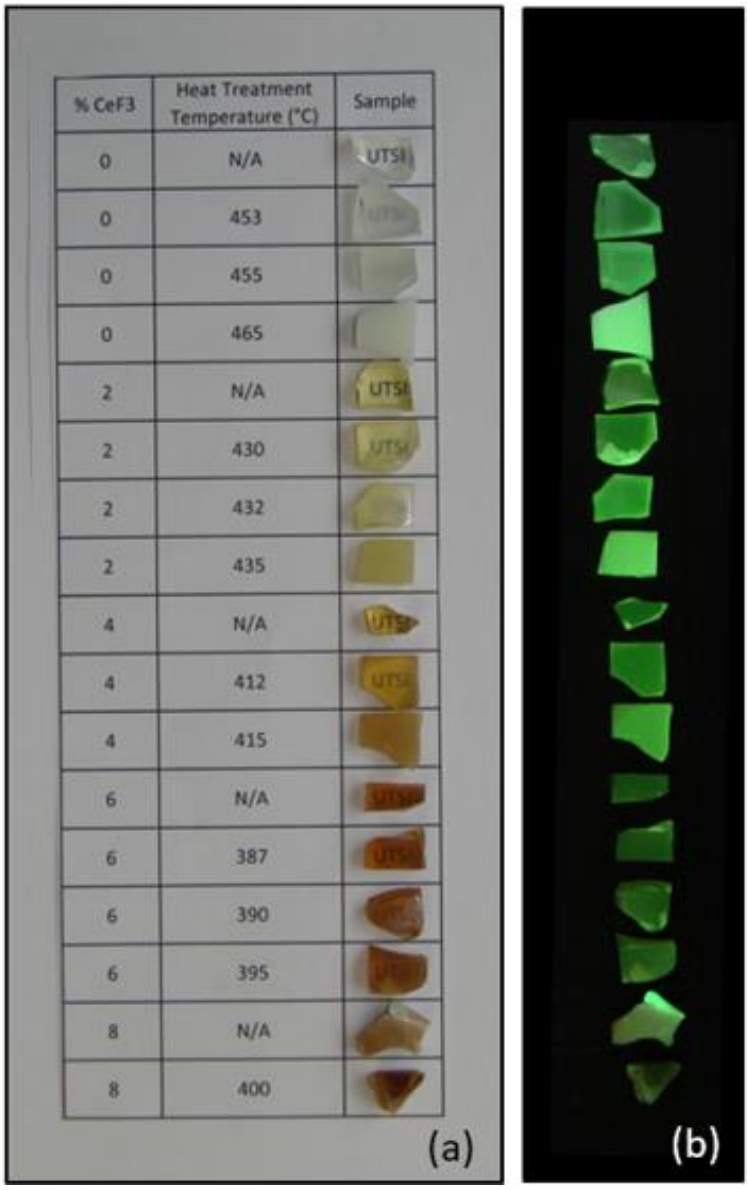

Fig 18. As-made and heat-treated samples under a) visible light and b) UV light

X-Ray Diffraction

The spectra of the as-made samples can be seen in Figure 19, with the characteristic peaks of CaF_2 being shown at the bottom (ICSD Col. 82707). No clear peaks can be seen in the 0-6% CeF_3 samples, while some very small peaks can be observed in the 8% CeF_3 spectrum. These small peaks line up with the peaks for CaF_2. In the 0-6% CeF_3 spectra, a very broad curve can be seen around 47 degrees two theta. The center of the curve roughly lines up with the peak for the (220) plane of CaF_2, which can indicate that there are CaF_2 crystallites present in the other samples. However, these crystallites are either too small or not concentrated enough for the detector to get a clear signal.

Figures 20, 21, 22, and 23 show the x-ray diffraction spectra for each composition. The trend is similar in each sample. There are no clear peaks in the as-made samples, only the broad curve that is centered on the peak of the (220) plane. At lower heat treatment temperatures, the only change that can be seen is the broad curve becoming more pronounced. At higher heat treatment temperatures, the CaF_2 peaks can be seen due to a sufficient amount of crystallization taking place.

Phosphorimetry

The emission spectra for the as-made samples excited at 273 nm can be seen in Figure 24. The primary peak of the terbium emission appears at 545 nm, with the secondary peak at 490nm, and the lesser peaks at higher wavelengths. The clear trend that can be observed is a loss in the intensity of the terbium emission as the amount of CeF_3 in the samples is increased. This trend disagrees with what was hypothesized. Two possible explanations can be found in literature [37-39]. The first is concentration quenching due to too much cerium being doped into the matrix. At higher dopant concentrations, the average distance between charged and uncharged electron traps will shrink, which can result in an increased probability of the trapped electrons tunneling to quenching sites. Another possibility is the oxidation of the Ce^{3+} into Ce^{4+}, which greatly facilitates the non-radiative transfer of energy back to the ground level.

The phosphorimetry results for each composition can be seen in Figures 25, 26, 27, and 28. The 0% CeF_3 sample was excited at 273 nm, while the 2-6% CeF_3 samples were excited at 296 nm due to these samples being more strongly excited at 296 nm than 273 nm. This shift in excitement intensity is likely due to the addition of CeF_3.The trends are similar for each composition. There is a sharp drop in luminescent intensity after heat treatment. The author posits that this drop may be due to absorption of the excitation energy by the CaF_2 crystals. Another trend of note is the slight recovery of the emission intensity after heat treatments at higher temperatures. This may be due to a greater amount of

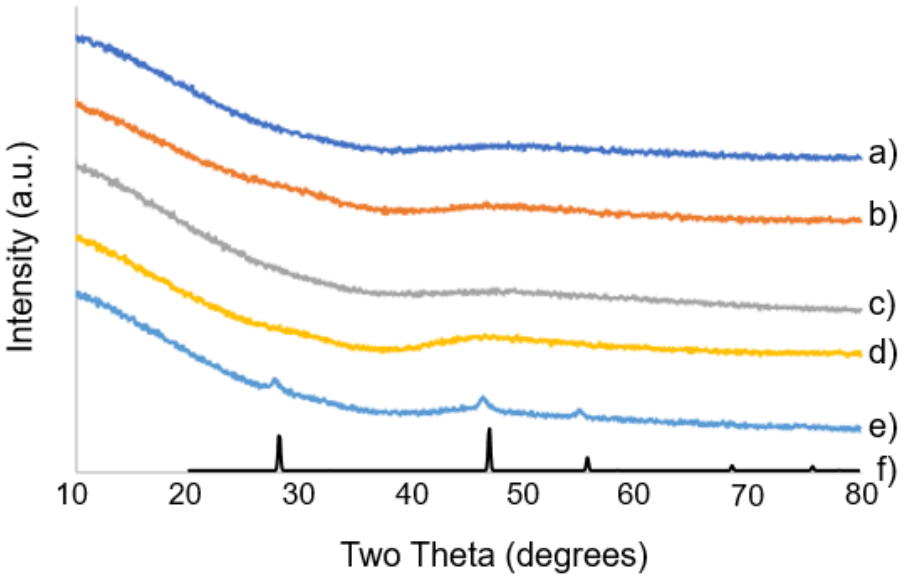

Fig 19. X-ray diffraction spectra for the as-made samples. a) 0% CeF_3, b) 2% CeF_3, c) 4% CeF_3, d) 6% CeF_3, e) 8% CeF_3, and f) ICSD col. 82707 (CaF_2)

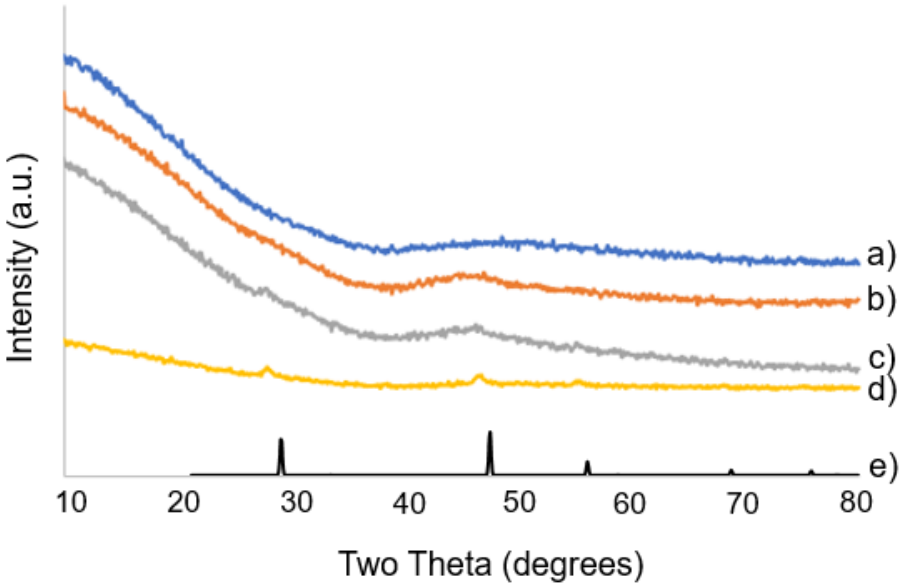

Fig 20. X-ray diffraction spectra for 0% CeF_3 samples. a) as-made, b) heat treated at 453°C, c) heat treated at 455°C, d) heat treated at 465°C, and e) ICSD col. 82707 (CaF_2)

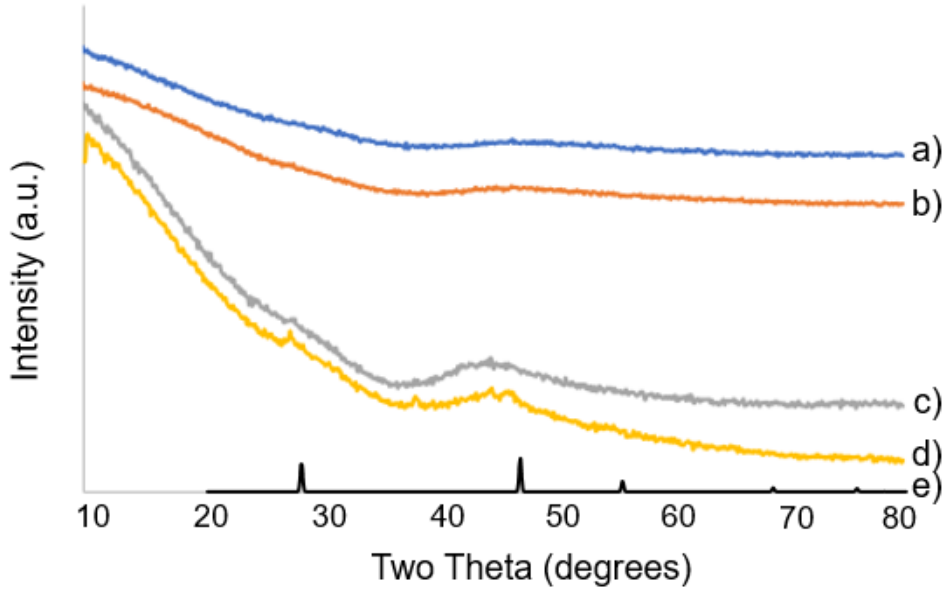

Fig 21. X-ray diffraction spectra for 2% CeF_3 samples. a) as-made, b) heat treated at 430°C, c) heat treated at 432°C, d) heat treated at 435°C, and e) ICSD col. 82707 (CaF_2)

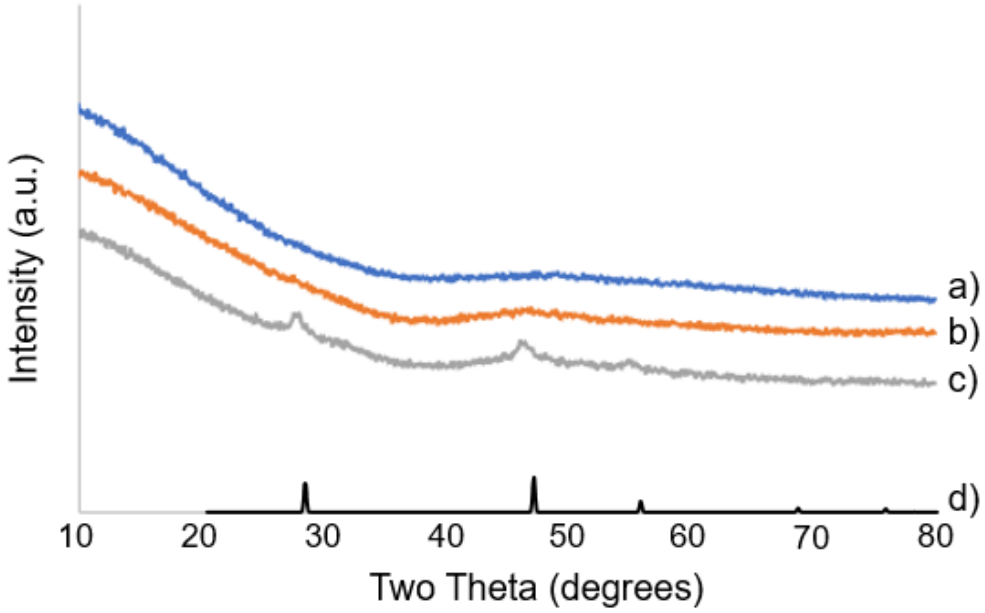

Fig 22. X-ray diffraction spectra for 4% CeF_3 samples. a) as-made, b) heat treated at 412°C, c) heat treated at 415°C, and d) ICSD col. 82707 (CaF_2)

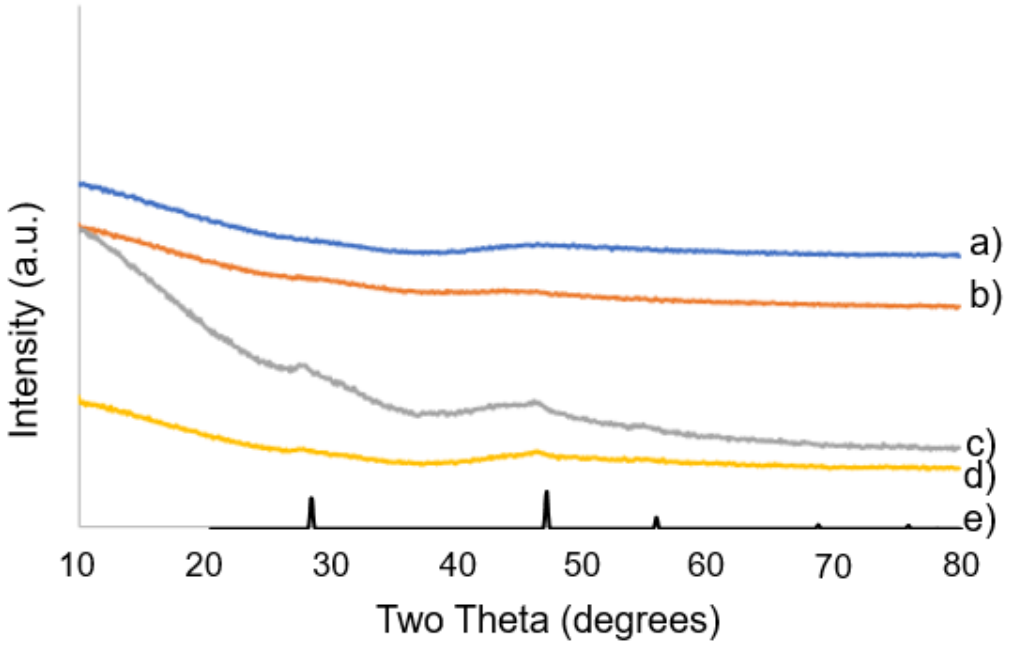

Fig 23. X-ray diffraction spectra for 6% CeF_3 sample. a) as-made, b) heat treated at 387°C, c) heat treated at 390°C, d) heat treated at 395°C, and e) ICSD col. 82707 (CaF_2)

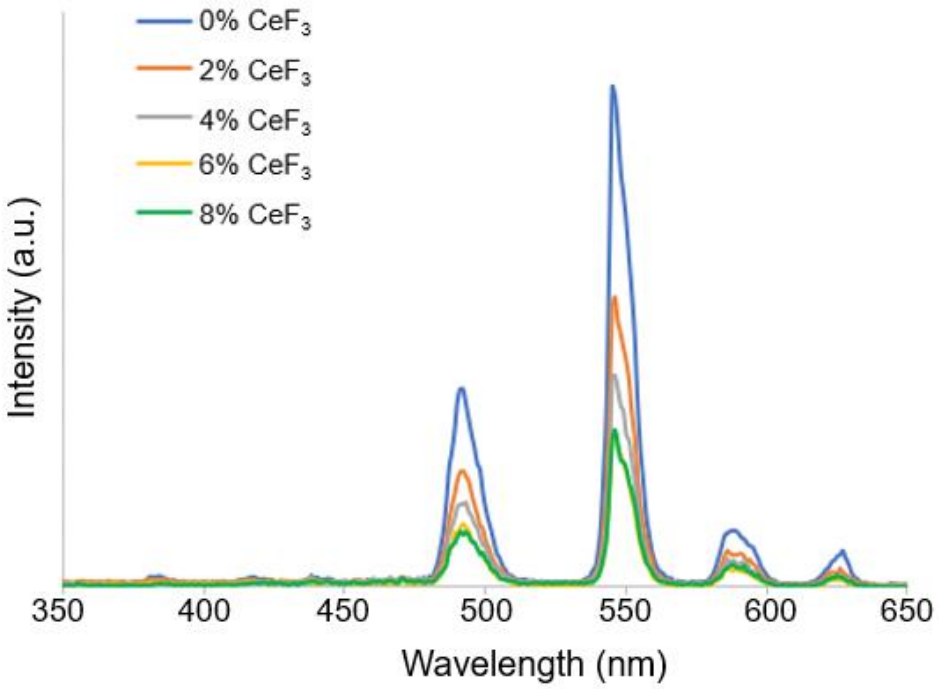

Fig 24. Emission spectra for the as-made samples at 273 nm excitation

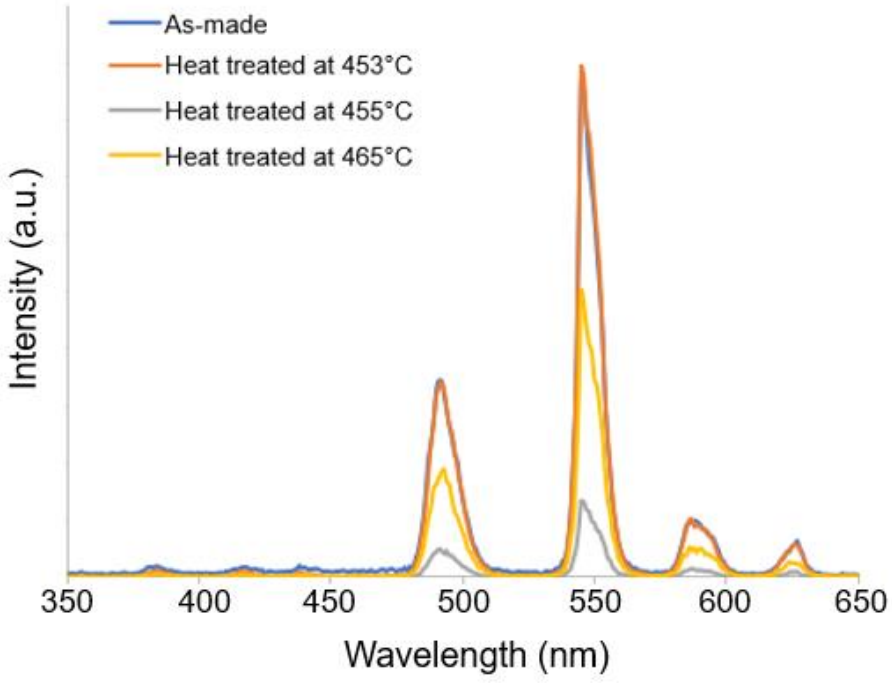

Fig 25. Emission spectra for the 0% CeF_3 samples at 273 nm excitation

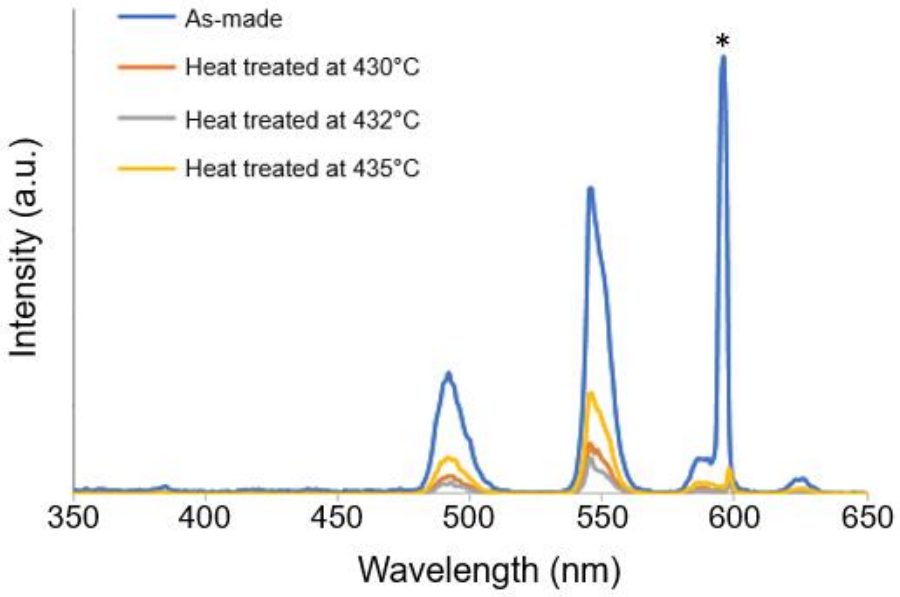

Fig 26. Emission spectra for the 2% CeF_3 samples at 296 nm excitation. "*" denotes an artifact caused by the excitation light

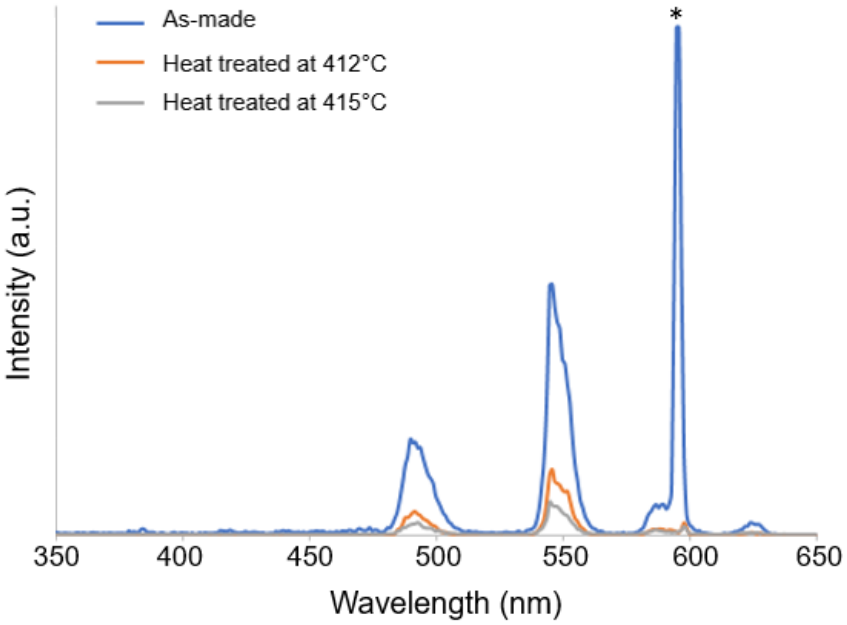

Fig 27. Emission spectra for the 4% CeF_3 samples at 296 nm excitation. "*" denotes an artifact caused by the excitation light

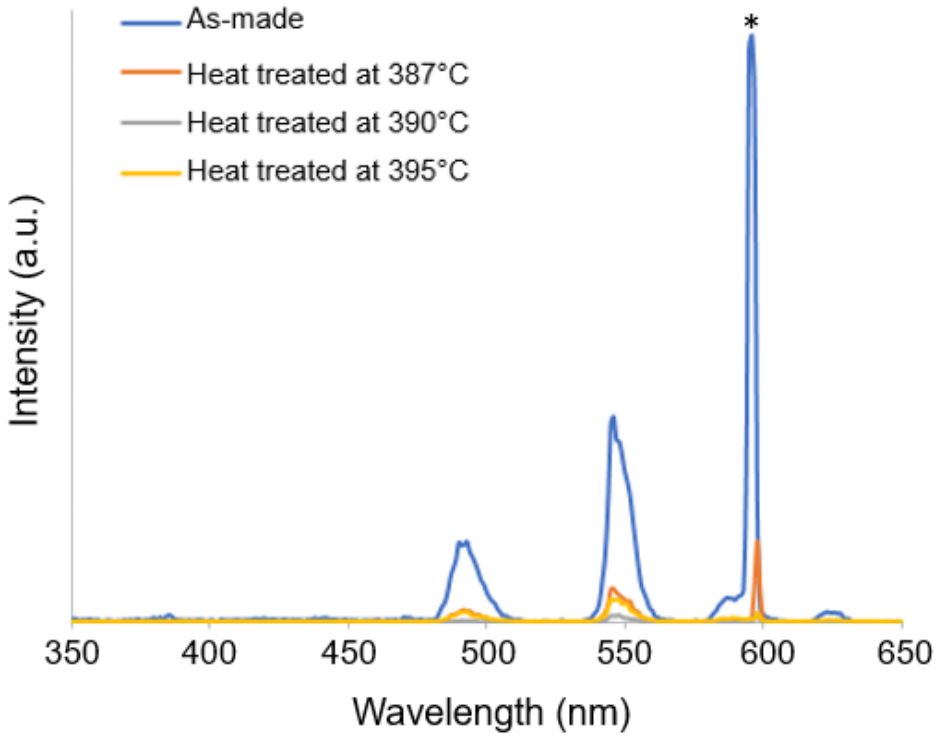

Fig 28. Emission spectra for the 6% CeF_3 samples at 296 nm excitation"*" denotes an artifact caused by the excitation light

scattering caused by the increased amounts of crystallization in those samples, which reduced the amount of light trapping.

Spectrophotometry

The spectrophotometry results for the as-made samples can be seen in Figure 29. The transmittance of the samples sharply declines with increased amounts of CeF_3. The series of valleys that can be observed in the spectra of the 0% CeF_3 sample are the various wavelengths of terbium, gadolinium, and cerium where their absorption is strongest. The dips at 255 nm, 377 nm, and 488 nm can be attributed to absorption from the Tb^{3+} ions [40, 41]. The dip at 350 nm can be attributed to Ce^{3+} absorption [41], while the dip at approximately 315 nm can be attributed to Gd^{3+} absorption [42]. The results for the 0%, 2%, 4%, and 6% samples can be seen in Figures 30, 31, 32, and 33. The 0% CeF_3 heat treated at 465°C and the 2% CeF_3 sample heat treated at 435°C were opaque and did not produce spectra. The transmittance can be seen to sharply drop after heat treatment in all samples, which is due to the scattering of the CaF_2 crystals.

X-Ray Scintillation Output

The x-ray scintillation results can be seen in Figure 34. The bar on the far right shows the brightness of a commercial scintillator. The two samples that had the highest intensity under x-ray excitation were the 0% CeF_3 sample that was heat treated at 465°C and the 2% CeF_3 sample that was heat treated at 435°C. These samples had an x-ray scintillation output of around 410 units, while the commercial scintillator had an x-ray scintillation output of 4110 units. An indirect detector using one of these glass-ceramic scintillators in place of the standard substrate would experience roughly a 10% increase in scintillation output.

Contrary to the emission spectra from UV excitation, the trend observed in the x-ray scintillation results shows only a slight overall decline in scintillation output as the amount of CeF_3 is increased. This gives a clear indication of the difference between UV and x-ray excitation and how a material emits under UV excitation is not necessarily a reflection of how it emits under x-ray excitation.

Conclusion

The luminescent intensity of the terbium was found to decrease with increasing amounts of CeF_3 when excited at 273 nm and 296 nm. This decrease was likely caused by either concentration quenching due to too much cerium being doped into the samples, or by the Ce^{3+} oxidizing to Ce^{4+}, which tends to facilitate the non- radiative transfer of energy. Either cause leads to less energy getting to the

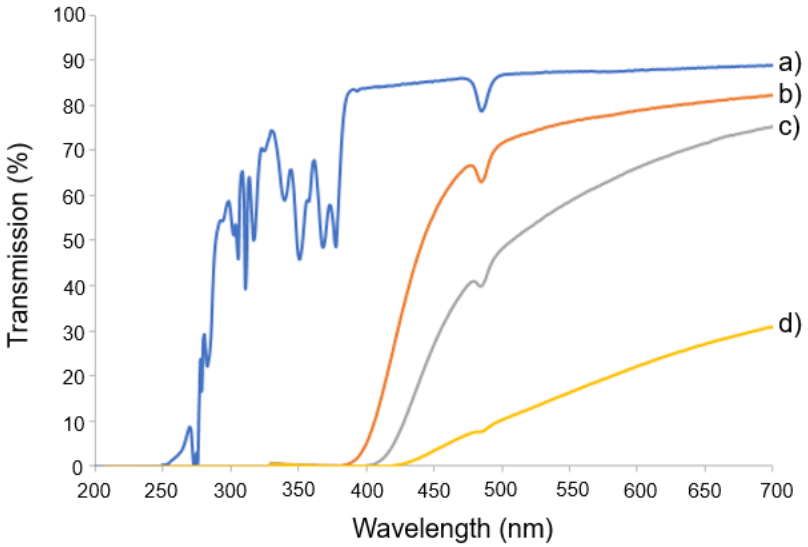

Fig 29. Transmission spectra for the as-made samples. a) 0% CeF_3, b) 2% CeF_3, c) 4% CeF_3, d) and 6% CeF_3

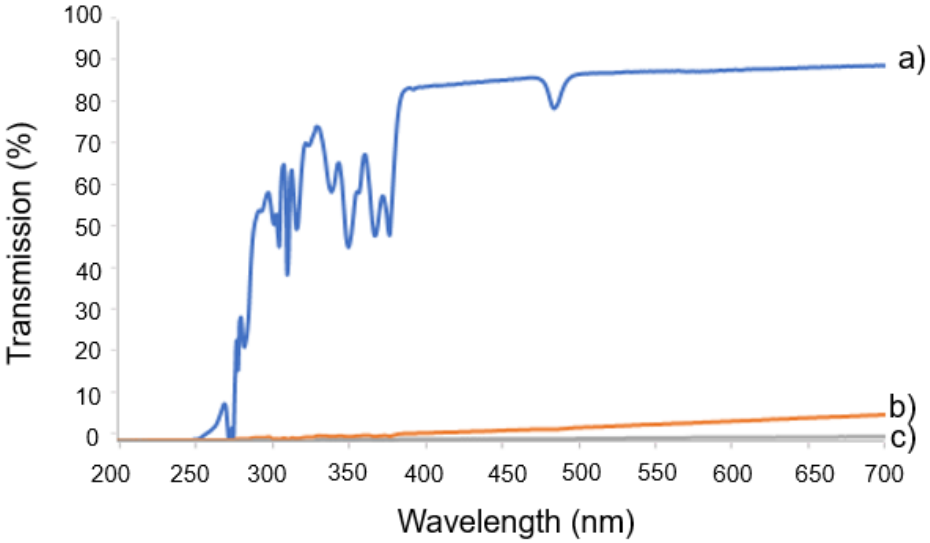

Fig 30. Transmission spectra for the 0% CeF_3 samples. a) as-made, b) heat treated at 453°C, and c) heat treated at 455°C

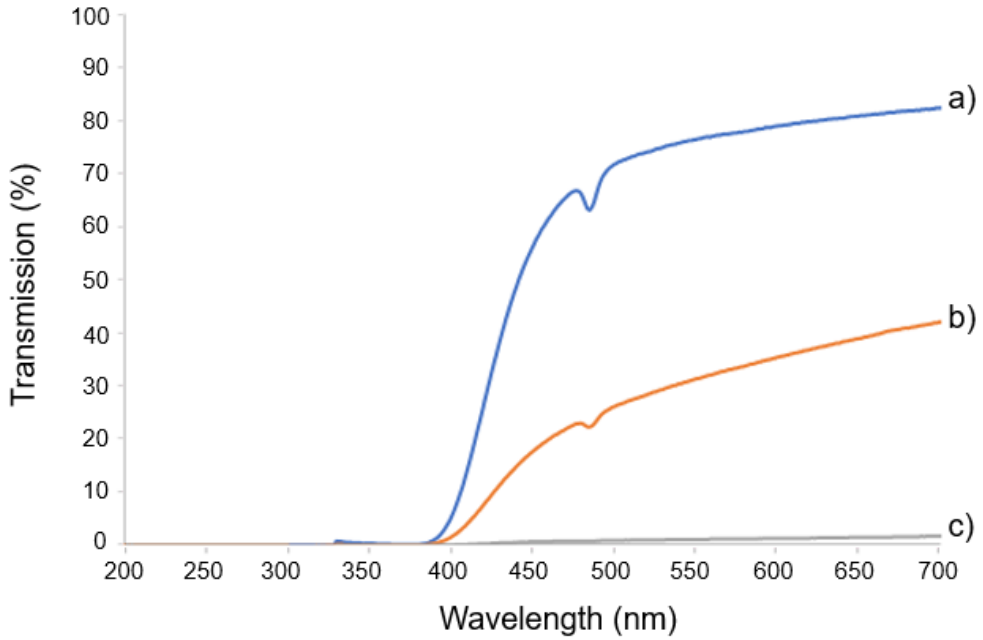

Fig 31. Transmission spectra for the 2% CeF_3 samples. a) as-made, b) heat treated at 430°C, c) and heat treated at 432°C

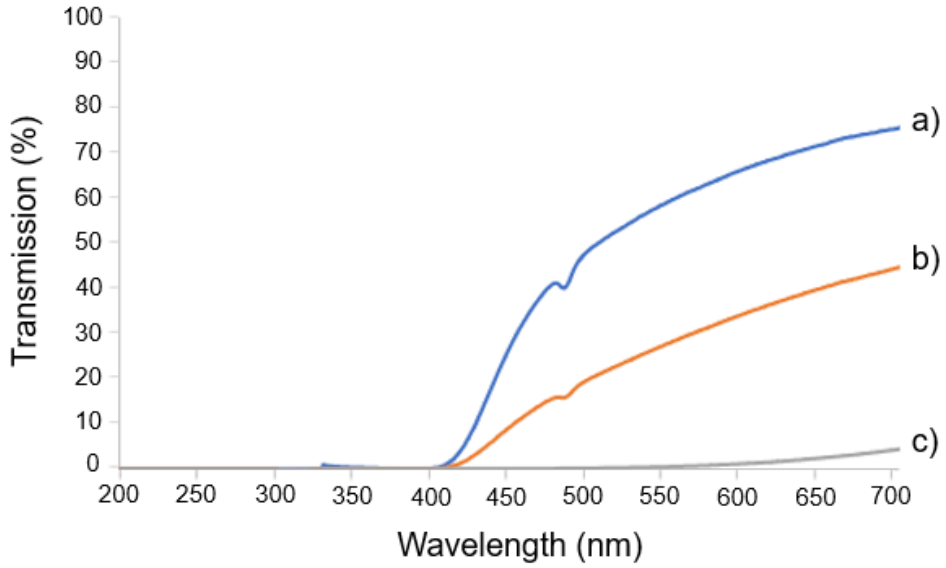

Fig 32. Transmission spectra for the 4% CeF_3 samples. a) as-made, b) heat treated at 412°C, and c) heat treated at 415°C

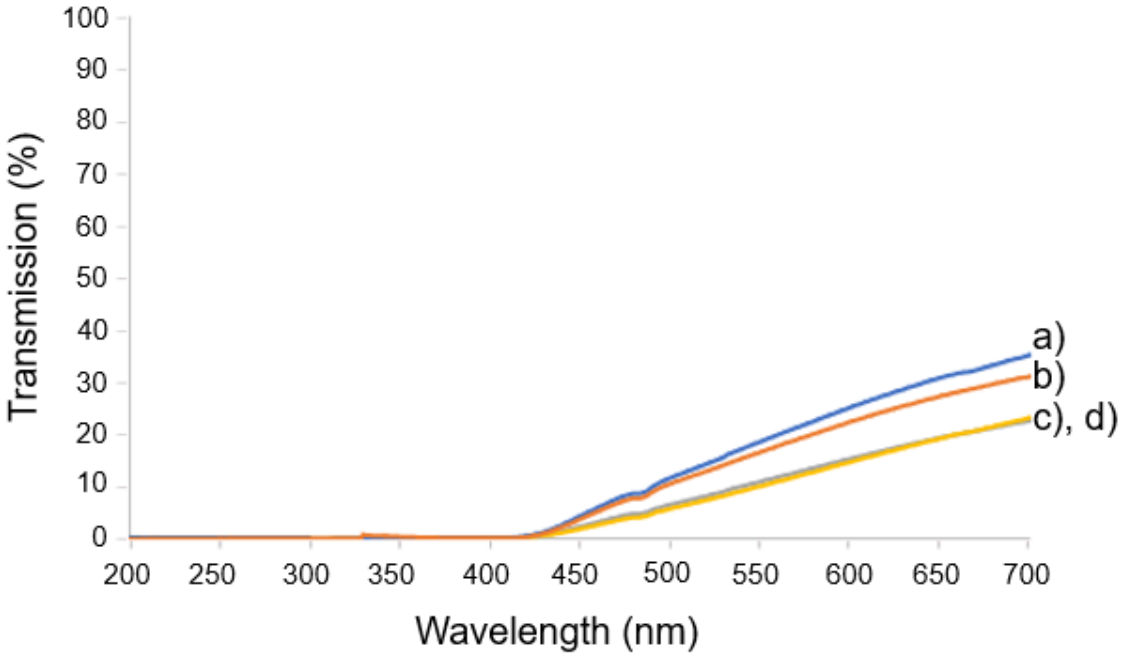

Fig 33. Transmission spectra for the 6% CeF_3 samples. a) as-made, b) heat treated at 387°C, c) heat treated at 390°C, and d) heat treated at 395°C. Note that there is significant overlap between the spectra of c) and d)

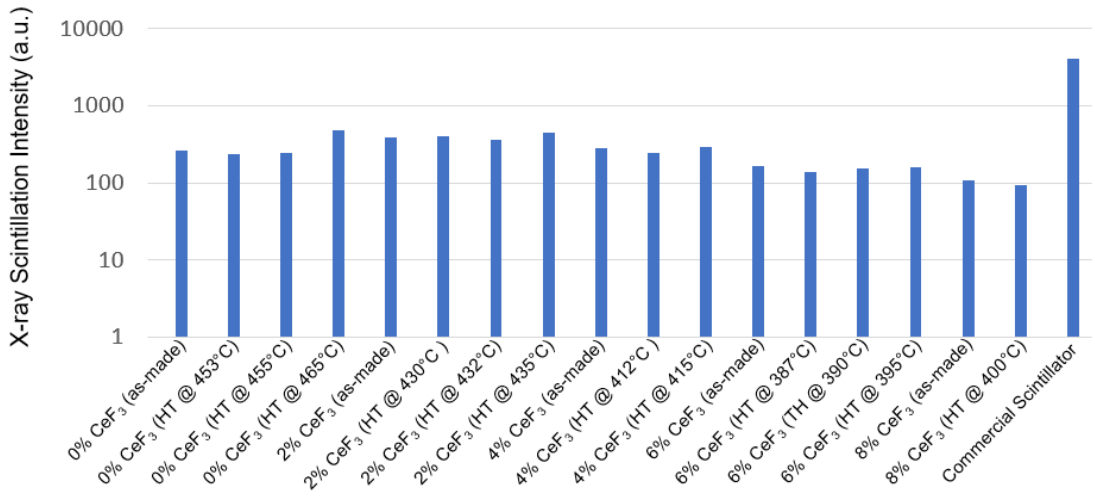

Fig 34. X-ray scintillation output of the samples and a commercial scintillator

terbium, which is what led to the decrease in emission intensity. The intensity was found to further decrease after heat treatments. This may be due to the transfer of energy to the terbium ions being hindered in some way by the CaF_2 crystals. The x-ray excitation results showed that the synthesized scintillators achieved an x-ray scintillation output that was roughly 10% that of a commercial scintillator. This change would lead to a significant increase in detector efficiency when paired with a bidirectional detector. When comparing the x-ray excitation results to the UV excitation results, there is a clear difference in the relative amount of loss in terbium emission as the amount of CeF_3 is increased. Under UV excitation the loss in relative intensity is severe, while under x-ray excitation the relative intensity is almost the same across all samples. The worst x-ray excitation results are those of the 8% CeF_3 samples, in which the loss in relative emission intensity may be due to how much more the CaF_2 crystals precipitated in those samples instead of the amount of CeF_3. In fact, the samples with 2% CeF_3 actually have a greater output than the 0% CeF_3 samples under x-ray excitation. These results show how the same material can emit differently depending on the excitation radiation.

Additional research will be required moving forward in order to better understand the energy transfer mechanisms between the cerium, gadolinium, and terbium. If the CeF_3 series were to be repeated, a lower amount of CeF_3 should be used in order to avoid concentration quenching. Going from 0% to 2% CeF_3 in 0.5% increments may be useful. Furthermore, a different crystalline component, perhaps lanthanum fluoride, should be used in order to investigate if the precipitation of the CaF_2 crystals had a negative effect on the terbium emission intensity. Photoelectron spectroscopy could be performed to detect the relative amounts of Ce^{3+} and Ce^{4+} in the samples, which may lead to further insight into the quenching mechanics of the cerium in these scintillators.

CONCLUSION

The results of the two series presented in this document show the high potential that glass-ceramic scintillators have for use as scintillating substrates in indirect digital radiography detectors. In the CaF_2 series, scintillators were synthesized in which the degree of scattering of the CaF_2 crystals was proportional to the amount of CaF_2, and CaF_2 crystals were precipitated and grown through the use of heat treatments. These results that the crystallization of CaF_2 can be controlled in glass ceramics and can be tailored to an ideal level of crystallization for scintillator applications. The relative luminescent intensity of the CaF_2 increased due to doping with Eu^{3+}, as well as shifted to a higher wavelength that is further into the visible spectrum, which makes it more useful for scintillator applications. These results show that doping with Eu^{3+} enhances the luminescence of CaF_2 and that scintillators containing these two dopants have potential for acting as a scintillating substrate for use in digital radiography detectors.

In the CeF_3 series, controlled precipitation and growth of the CaF_2 crystals was observed after heat treatment. Additionally, the detected luminescent intensity of the terbium decreased as the amount of CeF_3 was increased under UV excitation, while no clear trend was observed under x-ray excitation. The detected loss in terbium emission under UV excitation is due to either concentration quenching or the oxidation of Ce^{3+} to CeF^{4+} and the precipitation of the CaF_2 crystals appeared to cause further losses. The x-ray scintillation output of the samples decreased by less than an order of magnitude as the CeF_3 content is increased, while the output of the 2% CeF_3 samples was greater than that of the 0% CeF_3 samples. This suggests that some degree of cerium has a positive effect on the terbium emission under x-ray excitation. The two brightest samples had an x-ray scintillation output of roughly 10% that of the commercial scintillator. If used as a scintillating substrate with a bidirectional detector, this would lead to a significant improvement in detector efficiency. While the results seen in the UV emission spectra disagree with what was hypothesized, the x-ray scintillation output is more relevant to the proposed application and should be considered more important.

Both of these series show that the precipitation and growth of CaF_2 crystals can be controlled through the amount of CaF_2 used during synthesis and with heat treatments. Precision control over the degree of crystal growth allows for the crystalline component of scintillators to be fine-tuned for specific applications, excitation radiation, and dopants by maintaining a balance between scattering and self-absorption. Furthermore, the composition used in both series was able to successfully host different rare earth dopants. This composition can potentially be used as a flexible host material for a variety of scintillator applications that use various rare earth dopants.

In the future, it may be of interest to redo the CeF_3 series with several changes that may improve the intensity of the terbium emissions. To begin with, less CeF_3 should be used during synthesis. As the brightest samples were the 0% CeF_3 and 2% CeF_3 samples, a series ranging from 0-2% CeF_3 in 0.5% increments may show an optimum concentration of CeF_3 somewhere in that range. Additionally, a different crystalline component should be used in order to investigate whether or not the precipitation of the CaF_2 crystals had a negative effect on the terbium emissions. One compound that may be of interest is lanthanum fluoride.

References

[1] Yorkston J, Rowlands JA. Chapter 4. flat panel detectors for digital radiography. In: Van Metter RL, Beutel J, Kundel HL, editors. Handbook of medical imaging, volume 1. physics and psychophysics. Washington: SPIE; 2000: 223–313.

[2] Kabir MZ, Kasap S. Photoconductors for x-ray image detectors. In: Kasap S, Capper P, editors. Springer handbook of electronic and photonic materials. New York, NY: Springer Handbooks. Springer International Publishing; 2017:1125–47.

[3] Clover Learning. Digital Radiography System Explained (step by step). Youtube. 2019. https://www.youtube.com/watch?v=YzV1kovMjkI

[4] Nikl M., Scintillation detectors for x-rays, Meas. Sci. Techno. 2006; 17: R37-R54

[5] Brixner L.H., New x-ray phosphors, Mater. Chem. Phys. 1987; 253-281

[6] Ishii M. and Kobayashi M., Single crystals for radiation detectors, Prog. Cryst. Growth Charact. 1992; 245-311

[7] Nikl M., Wide band gap scintillation materials. Progress in the technology and understanding. Phys. Status Solidi 2000; 595-620

[8] Wojtowicz A.J., Rare-earth-activated wide bandgap materials for scintillators, Nucl. Instrum. Methods Phys. Res. A 2002; 201-207

[9] Weber M.J., Inorganic Scintillators: today and tomorrow, J. Lumin. 2002; 34-45

[10].van Eijk C. W. E., Inorganic scintillators in medical imaging, Phys. Med. Biol 2002; R85-R106

[11] Swank RK. Absorption and noise in x-ray phosphors. J Appl Phys. 1973;44(9):4199–4203.

[12] Lubberts G. Random noise produced by x-ray fluorescent screens. Journal of the Optical Society of America. 1968;58(11):1475–1483.

[13] Boone JM. X-ray production, interaction, and detection in diagnostic imaging. In: Van Metter RL, Beutel J, Kundel HL, editors. Handbook of medical imaging, vol. 1. physics and psychophysics. SPIE: Washington; 2000: 1–78.

[14] Weisfield RL. Amorphous silicon tft x-ray image sensors. In: International Electron Devices Meeting Technical Digest (Cat. No.98CH36217): 1998.

[15] SA, Wickersheim KA. X-ray exposure reduction using rare-earth oxysulfide intensifying screens. Radiology. 1972;105(1):185–190

[16] Kuo Y., Thin Film Transistors. 1. Amorphous silicon thin film transistors. 2004: Kluwer Academic Publishers

[17] Lee G, Savage NB, Wagner B, Zhang Y, Jacobs B, Menkara H, et al. Synthesis and luminescence properties of transparent nanocrystalline GdF3: Tb glass-ceramic scintillator. J Lumin. 2014;147:363–366.

[18] Appleby GA, Bartle CM, Williams GVM, Edgar A. Lithium borate glass ceramics as thermal neutron imaging plates. Curr Appl Phys. 2006;6(3):389–392.

[19] Wang Q, Yang B, Zhang YP, Xia HP, Zhao TC, Jiang HC. High light yield Ce^{3+}-doped dense scintillating glasses. J Alloy Compd. 2013;581:801–804

[20] Sidebottom DL, Hruschka MA, Potter BG, Brow RK. Increased radiative lifetime of rare earth-doped zinc oxyhalide tellurite glasses. Appl Phys Lett. 1997;71(14):1963–1965

[21] Struebing C, Beckert MB, Nadler JH, Kahn B, Wagner B, Kang Z. Optimization of a gadolinium-rich oxyhalide glass scintillator for gamma ray spectroscopy. J Am Ceram Soc. 2018;101(3):1116–1121

[22] Leonard R.L., Johnson JA. Scintillator glasses. In: Musgraves JD, Hu J, Calvez L, editors. The springer handbook of glass, handbook section: optical and photonic applications. Cham, Switzerland: Springer Nature Switzerland; 2002: 1555–1584.

[23] Leonard R. L., et al. Scintillating glass-ceramic substrates for indirect flat panel detectors in digital radiography. J Am Ceram Soc. 2020;103:6893-6900

[24] Greve DW. Thin-film transistors. In: Buschow KHJ, Cahn RW, Flemings MC, Ilschner B, Kramer EJ, Mahajan S, Veyssière

[25] Zhanjun L., et al., Nanoscale “fluorescent stone”: Luminescent Calcium Fluoride Nanoparticles as Theranostic Platforms, Theranostics. 2016; 2380-2393

[26] Rodnyi P., Physical Processes in Inorganic Scintillators, St. Petersburg State Technical University, CRC Press (1997)

[27] Alharbi N.D., Size Controlled CaF_2 Nanocubes and Their Dosimetric Properties Using Photoluminescence Technique, Journal of Nanomaterials Vol.15. 2015; 1-9

[28] Smet P., Avci N., den Eeckhout K.V., and Poelman D., Extending the afterglow in $CaAl_2O_4$:Eu,Nd persistent phosphors by electron beam annealing, Optical Materials Express (2012)

[29] Mares J.A., et al., Optical Studies of Ce^{3+} Doped Gadolinium Aluminum Perovskite Single Crystals, Chemical Physical Letters Vol. 206. 1993; 9-14

[30] Gyuhyon L., et al., Synthesis and Luminescence properties of GdF_3:Tb glass-ceramic scintillator, J Lumin Vol 147. 2014; 363-366

[31] Jain N., et al., Synthesis and Rational design of Europium and Lithium Doped Sodium Zinc Molybdate with Red emission for Optical Imaging, Scientific Reports Vol. 9 (2019)

[32] Steinbach C.O., Ujhelyi F., and Lorincz F., Measuring the Optical Scattering Length of Scintillator Crystals, IEEE Transactions on Nuclear Science Vol. 61. 2014; 2456-2463

[33] Rajagukguk J, et al. Structural and optical characteristics of Eu^{3+} ions in sodium-lead-zinc-lithium-borate glass system. Journal of Molecular Structures. 2016; 1121: 180-187.

[34] Howansky A, Mishchenko A, Lubinsky AR, Zhao W. Comparison of CsI: Tl and Gd_2O_2S: Tb indirect flat panel detector x-ray imaging performance in front- and back-irradiation geometries. Med Phys. 2019;46(11):4857–68.

[35] Howansky A, Lubinsky AR, Suzuki K, Ghose S, Zhao W. An apparatus and method for directly measuring the depth-dependent gain and spatial resolution of turbid scintillators. Med Phys. 2018;45(11):4927–41.

[36] Lubinsky A, Howansky A, Zheng H, Zhao W. Back-irradiated and dual-screen sandwich detector configurations for radiography. J Med Imag. 2019; 6(3):039801.

[37] Blasse G. Luminescent materials: is there still news? Journal of Alloys and Compounds. 1995; 225: 529-533

[38] Blasse G., Schipper W., and Hamelink J. J. On the quenching of the luminescence of the trivalent cerium ion. Inorganic Chimica Acta. 1991; 189: 77-80

[39] Lakshminarayana G., et al. Structural, thermal, and luminescence properties of cerium-fluoride-rich oxyfluoride glasses. Optical materials. 2012; 35: 117-125

[40] Beckert M. et al. Meidcal imaging scintillators from glass-ceramics using mixed rare-earth halides. Optical Materials. 2016; 60:513-520

[41] Dong-Bing H.E., Chun-Lei Y.U., Ji-Meng C., Shun-Guang L.I., and Li-Li H.U. A Novel Ce^{3+} /Tb^{3+} Codoped Phosphate Glass as Down-Shifting Materials for Enhancing Efficiency of Solar Cells. Chi. Phys. Lett. 2010; 27(11) 114208: 1-4

[42] Wang Q. et al. High light yield Ce^{3+} -doped dense scintillating glasses. Journal of Alloys and Compounds. 2013; 581: 801-804

VITA

Austin M. Thomas was born in Winterport, Florida. He lived in various states across the United States as he grew up, due to his father being a member of the U.S. Navy. After his father's retirement, Austin attended high school in Knoxville, Tennessee. He went on to attend the University of Tennessee, Knoxville and received Bachelor of Science in Materials Science and Engineering. Austin spent the year after graduation working for a solar power company, before deciding to return to school. He chose to attend the University of Tennessee Space Institute, where he earned his MS in Biomedical Engineering in 2021 and will work towards a Doctor of Philosophy degree in Mechanical Engineering. After graduation, Austin will pursue a career in industry.